MRS Energy & Sustainability (2022) 9:106–128

doi:10.1557/s43581-022-00033-z

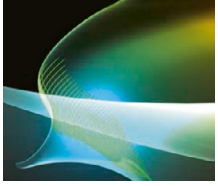

LARGE-SCALE ENERGY STORAGE -- REVIEW

Advanced aqueous batteries: Status and challenges

Jin Yi, Institute for Sustainable Energy/College of Sciences, Shanghai University, Shanghai 200444, China

Yongyao Xia, Department of Chemistry and Institute of New Energy, Fudan University, Shanghai 200433, China

Address all correspondence to Yongyao Xia at yyxia@fudan.edu.cn

(Received: 2 December 2021; accepted: 25 May 2022;
published online: 11 July 2022)

ABSTRACT

The status for advanced aqueous batteries are summarized in detail. The challenges for the application of aqueous batteries are discussed.

The electricity grids with high stability and reliability require a desired balance of energy supply and demand. As the typical sustainable energy, the intermittent solar and wind would result in electricity grid instability. Aqueous batteries have been considered to be appealing stationary power sources for sustainable energy. Advanced aqueous batteries can address the safety concern derived from the employment of highly toxic and flammable organic solvents in lithium-ion batteries together with the poor cycle life presented in commercialized aqueous rechargeable batteries. This review will introduce several kinds of newly developed aqueous batteries, including aqueous Li (Na)-ion batteries, zinc anode-based batteries (Zn-metal oxide, Zn-air, Zn–Br_2, and Zn–$Ni(OH)_2$ batteries), and $Ni(OH)_2$ cathode-based batteries ($Ni(OH)_2$–MH and $Ni(OH)_2$-organic composite batteries). The materials, mechanisms, and battery techniques for the above aqueous batteries will be introduced in detail. The status and challenges for the application of aqueous batteries will also be discussed.

Keywords energy storage · Li · Na · Zn · Ni

Discussion

The aqueous batteries are considered as the promising large-scale energy storage systems. However, the narrow voltage window of aqueous electrolyte limits the electrochemical performance of aqueous batteries. Moreover, the instabilities of electrode materials in aqueous electrolyte further hamper the practical application of aqueous batteries. Consequently, large efforts involving scientific and technical communities are required to be devoted with the aim to facilitate the development of aqueous batteries.

Introduction

With the rapid development of economy and society, the energy demand has become more and more urgent. The increasing depletion of traditional non-renewable resources, such as coal, oil, and natural gas, and the resulting environmental pollution and energy crisis are widely concerned. The exploitations of wind energy, solar energy, and new energy technologies become significant.[1–6] The development of energy-saving and new energy vehicles taking the place of traditional fuel vehicles would be an effective way to save petroleum resources and reduce harmful emissions from vehicles. In order to satisfy the application of large-scale power battery, the desired batteries are expected to not only achieve excellent electrochemical performance but also take into account the requirements of low cost and high safety.[7–11] The development of advanced aqueous batteries based on aqueous electrolytes can greatly enhance the safety of batteries and reduce the cost and the environmental pollution caused by organic solvents. At the same time, the high ionic conductivities of aqueous electrolyte can enable to achieve high power density.[12–15] Therefore, the advanced aqueous battery has been regarded as the next generation of energy storage system (ESS). In the past decades, several advanced aqueous batteries have been developed.[16–20] Among them, aqueous Li (Na)-ion batteries, zinc anode-based batteries, and $Ni(OH)_2$ cathode-based batteries are considered as the competitive candidate. In this review, the status and challenges of the advanced aqueous batteries are summarized, and the promising strategies are provided.

Status of advanced aqueous batteries

Aqueous Li (Na)-ion batteries

Aqueous Li (Na)-ion batteries are potential candidates for large-scale ESSs, which would resolve the challenges of Li-ion battery derived from the organic electrolytes, such as flammability, strict manufacturing conditions, and high price. Generally, the liquid electrolytes are prepared through dissolving salt in a suitable solvent. Compared to non-aqueous solvents, water is a wonderful alternative because it has intrinsic safety and high number of acceptors and donors. The ionic conductivity of aqueous electrolyte is usually an order of magnitude higher than that of the non-aqueous electrolyte at a given concentration, subsequently, a high-power aqueous storage system can be realized. However, the aqueous electrolyte presents a small voltage window of 1.23 V, which limits the applications of lithium-ion batteries (ALIBs) and sodium-ion batteries (ASIBs). Meanwhile, the redox potentials of electrode materials for aqueous batteries are required to be within the electrolysis potentials of H_2O, beyond which the H_2O decomposition will be carried out accompanying with the H_2/O_2 evolution. Additionally, the co-insertion of protons into host electrode materials and the dissolution of electrodes play a significant role in the electrochemical performance, which are dependent on the pH of electrolyte and the stabilities of cathode material. Thus, in the following section, the status and challenges of ALIBs and ASIBs will be discussed in detail.

Aqueous Li-ion battery

In 1994, the first ALIB prototype is proposed by Dahn and co-workers, which are composed of $LiMn_2O_4$ and VO_2 as cathode and anode, respectively.[21] However, the electrochemical window of aqueous electrolytes is limited due to the low potential of water decomposition. Several proposed electrode active materials for ALIBs are developed.[22–25] The cathode materials for ALIB, such as $LiFePO_4$, $LiMn_2O_4$, and $LiCoO_2$, show the intercalation potential between 3 and 4 V vs Li^+/Li.[26–29] The intercalation can be conducted before oxygen evolution according to the relationship among the hydrogen evolution potentials, oxygen evolution potentials, and pH value (Fig. 1). Anode materials with intercalation potential between 2 and 3 V vs. Li^+/Li can be selected for ALIB. In theoretical, a lithium-accepting material with a lower potential can serve as anode, and lithium source material with a higher potential can function as cathode in an ALIB, whose working voltage is required in the range of O_2/H_2 evolution potential. Generally, the ALIB is operated in the presence of both H_2O and O_2, and the following reaction would take place (Eq. 1):

$$\text{Li(intercalated)} + (1/4)O_2 + (1/2)H_2O \leftrightarrow Li^+ + OH^-. \quad (1)$$

The potential of a lithium intercalation compound, $V(x)$, can be determined by the below equation:

$$V(x) = 4.268 - 0.059\ \text{pH(V)}. \quad (2)$$

It is shown that no materials can function as anode for ALIB at aerobic condition based on Eq. 2, no matter what pH of the electrolyte is. At pH 7 and pH 13, the equilibrium voltage is calculated to be 3.85 and 3.50 V vs. Li^+/Li, respectively, which is higher than the lithium-ion intercalation potential (below 3.0 vs. Li^+/Li) of anodes for ALIB. Unfortunately, all anode materials sustain the chemical oxidization driven by the O_2 and H_2O at the reduction state, which would replace the electrochemical redox process. Thus, it is necessary to eliminate oxygen for ALIB technology.

The protons can be detected in the lattice of cathode, such as delithiated layered $Li_{1-x}Ni_{1/3}Mn_{1/3}Co_{1/3}O_2$, and $Li_{1-x}CoO_2$, when lithium is extracted deeply at a low pH electrolyte. However, the phenomenon is not observed in olivine $Li_{1-x}FePO_4$ and spinel $Li_{1-x}Mn_2O_4$. The issue of proton insertion can be solved by adjusting the potential for proton intercalation through modulating the pH of electrolyte. As an example, it is possible to obtain stable lithium-ion intercalation for $LiCo_{1/3}Ni_{1/3}Mn_{1/3}O_2$ cathode in electrolyte with pH over 11 as well as make the achievement of lithium-ion intercalation for $LiCoO_2$ in pH 9 solution.[30,31] In addition, the cycling ability of ALIB would be limited due to the soluble issue of electrode materials in water. Especially, the dissolution of cathode material would be affected by its surface area. As for example, the large surface area is usually presented for the typical vanadium oxides prepared at low temperature, including VO_2, LiV_3O_8, and LiV_2O_5. Therefore, it is apt to select electrode materials with small specific surface

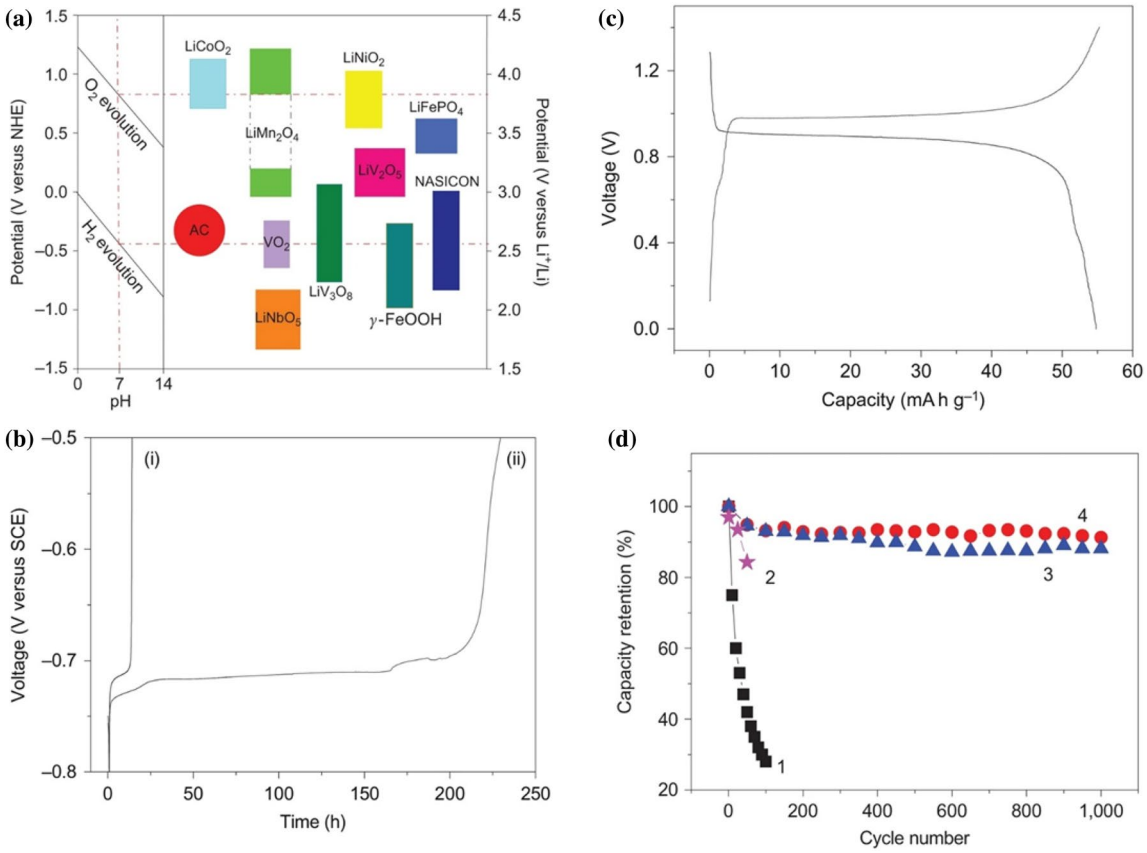

Figure 1. (a) The relationship between intercalation potential and pH value. (b) The self-discharge curves of $LiTi_2(PO_4)_3$ with/without O_2. (c) The typical charge/discharge profiles of $LiTi_2(PO_4)_3/LiFePO_4$ ALIB in 1 M Li_2SO_4 without O_2. (d) The cycle life of $LiTi_2(PO_4)_3/LiFePO_4$ ALIB at various pH and with/without O_2.[1] Adapted from Ref [1].

area. In addition, it is effective to utilize coating technology to enhance the stability of electrode materials in aqueous electrolytes.[25] Although $LiFePO_4$ suffers from decomposition in strong alkaline solution, it can be hampered through carbon coating.

Thermodynamically, a stable electrochemical window of 1.23 V is shown in aqueous electrolyte, which can expand the stability limit to 2 V by kinetic effects. For example, an output voltage of 2.0 V is delivered in Pb-acid batteries. It is suggested to pay attention to the reactions in aqueous electrolyte involving H_2/O_2 evolution, which would change the capacity of the electrode materials. Impressively, the H_2/O_2 evolution side reaction cannot be inhibited at full charge process owing to the intrinsic potential of lithium-ion intercalation in electrode. When employing the Fe- or Mn-based oxide as cathode, the intensity of metal ion field significantly impacts the O_2 reduction and evolution, which would be resulted from the electrostatic behavior of O_2 and OH^- absorption on the active site.[32] Highly oxidized redox couples are delivered in Fe and Mn ion, which serve as the active site for O_2 reduction and evolution side reactions.[33] In addition to the ion field intensity, the morphology of these cathode also plays a vital role on O_2 reduction and evolution. Thus, it is promising to decrease the inductive effect between transition metal ion and oxygen atom, which can inhibit the O_2 reduction and evolution. Moreover, it is required to keep a balance between the side reaction and energy storage owing to the positive effect by the porous or core–shell morphology. The stability of electrode materials would be reduced due to the presence of H_2/O_2 evolution reactions, which can change the pH value at the vicinity of electrode. As it is well known, organic electrolyte can be also decomposed in lithium-ion batteries during full charge process. A protective layer (SEI film) can be formed by the decomposition of organic electrolyte on the surface of electrode. Side reactions can be further reduced under the protection of SEI film. Unfortunately, the SEI film would not be formed to protect electrode owing to the gaseous products (H_2/O_2) originating from the decomposition of aqueous electrolyte. Hence, it is significant to adjust the working potential of cathode and anode for ALIB.[34] The stabilities of electrode materials in aqueous electrolytes have been extensively analyzed by our group, and it is found that the anodes of ALIB can be typically self-discharged in a discharged state due to the chemical oxidization with O_2. The stability of electrode can be improved via allaying oxygen. A high capacity retention (over 90% after 1000 cycles) is presented for $LiTi_2(PO_4)_3/Li_2SO_4/LiFePO_4$ ALIB after fully charge/discharge in 10 min, and the capacity retention of 85% after 50 cycles is exhibited even at a very low current rate

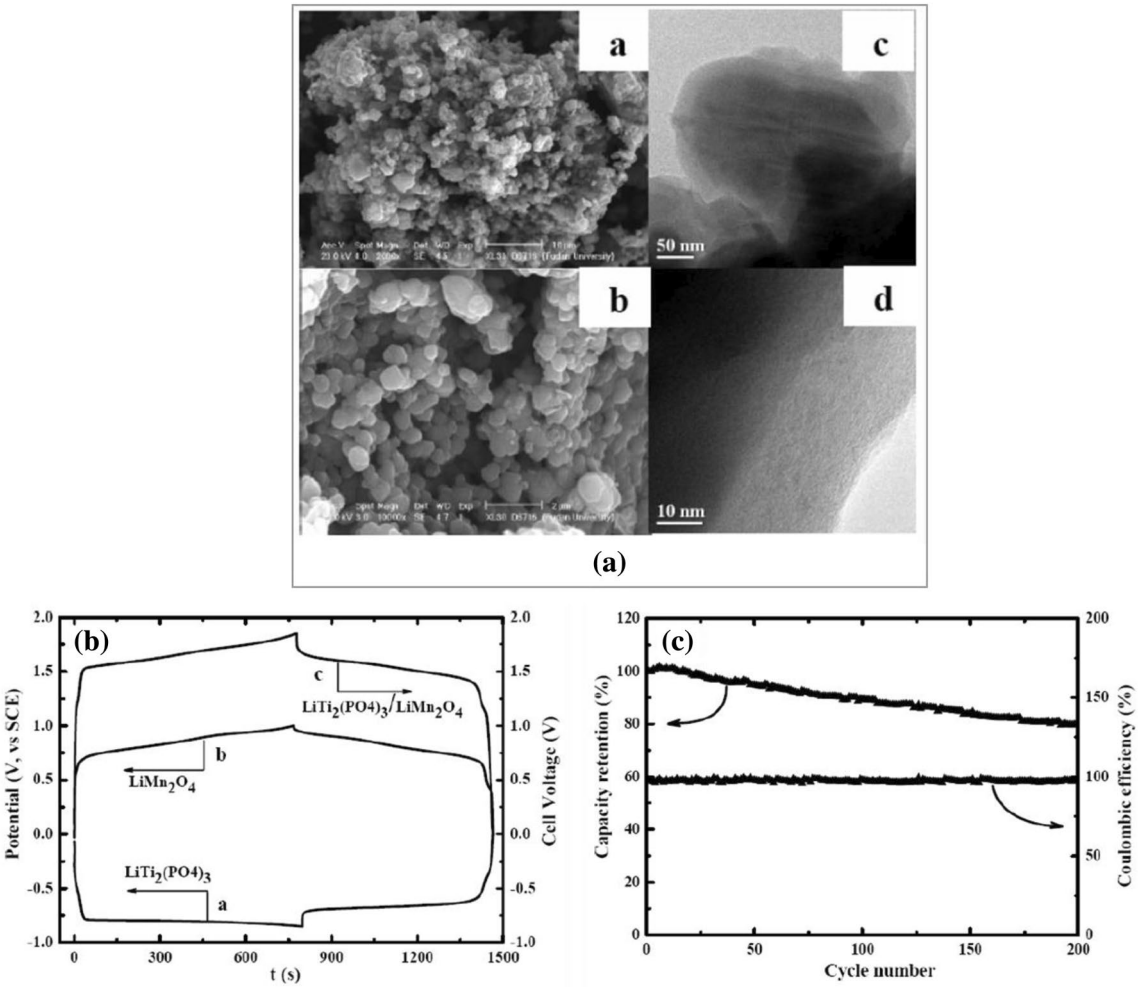

Figure 2. (a) The SEM and TEM images of carbon-coated $LiTi_2(PO_4)_3$. (b) The typical charge/discharge curves of $LiTi_2(PO_4)_3$, $LiMn_2O_4$ and a composite voltage profile of ALIB based on $LiTi_2(PO_4)_3/LiMn_2O_4$. (c) The cycle life of $LiTi_2(PO_4)_3/LiMn_2O_4$ ALIB.[25] Adapted from Ref [25].

(~ 0.125 C) (Fig. 1).[1] Thus, it is promising to offer an energy storage system, which endows low cost, long cycle life, high safety, and appropriate energy density. Furthermore, it is a key issue to restrain the oxygen evolution under charge or overcharge conditions, which would improve the electrochemical performance of ALIB. To solve the above issue, carbon coating technology can be employed to improve the capability and cycling stability of electrochemical active materials, which is demonstrated by the subsequent studies. An average operating voltage of 1.5 V, a specific energy of 60 Wh kg^{-1}, and high capacity retention of 82% are exhibited using the carbon-coated $LiTi_2(PO_4)_3$ and $LiMn_2O_4$ as anode and cathode in aqueous electrolyte, respectively (Fig. 2).[25]

Although the limitation of H_2/O_2 evolution reactions can be achieved via adjusting the pH value of electrolyte, the electrochemical stability window of electrolyte is still narrow. The SEI film can effectively protect electrode from side reactions; however, it cannot be formed in dilute aqueous solution. Subsequently, the concept of "water in salt" electrolyte is proposed that a dense interphase can be produced on the anode surface driven by anion reduction.[35] The electrochemical stability window scales with the Lithium bis(trifluoromethane sulfonyl) imide (LiTFSI) concentration that both oxygen and hydrogen evolution potentials are expanded. The hydrogen evolution is inhibited through a passivation process originating from the LiTFSI reduction. The oxygen evolution is suppressed by reducing the electrochemical activity of water. LiTFSI shows an extremely high concentration (> 20 M) in aqueous solution, revealing a wide electrochemical window (~ 3.0 V). In the ALIB based on $LiMn_2O_4$ and Mo_6S_8 as cathode and anode, respectively, nearly 100% coulombic efficiency is delivered after 1000 cycles at 0.15 and 4.5 C, respectively. The hydrated Li ion is formed in dilute aqueous electrolyte; whereas, anions instead of certain water are involved in the solvation sheath. Moreover, LiF-based SEI film is observed on Mo_6S_8 surface, which is generated by the $TFSI^-$ anion reduction; subsequently, the stability of electrode is effectively enhanced (Fig. 3). Compared with water, $TFSI^-$ interacting with Li^+ prefers to be reduced to form a dense interphase on electrode. Thus, the enlarged stability of electrode and wide electrochemical stability window can be obtained when employing the water-in-salt electrolyte.

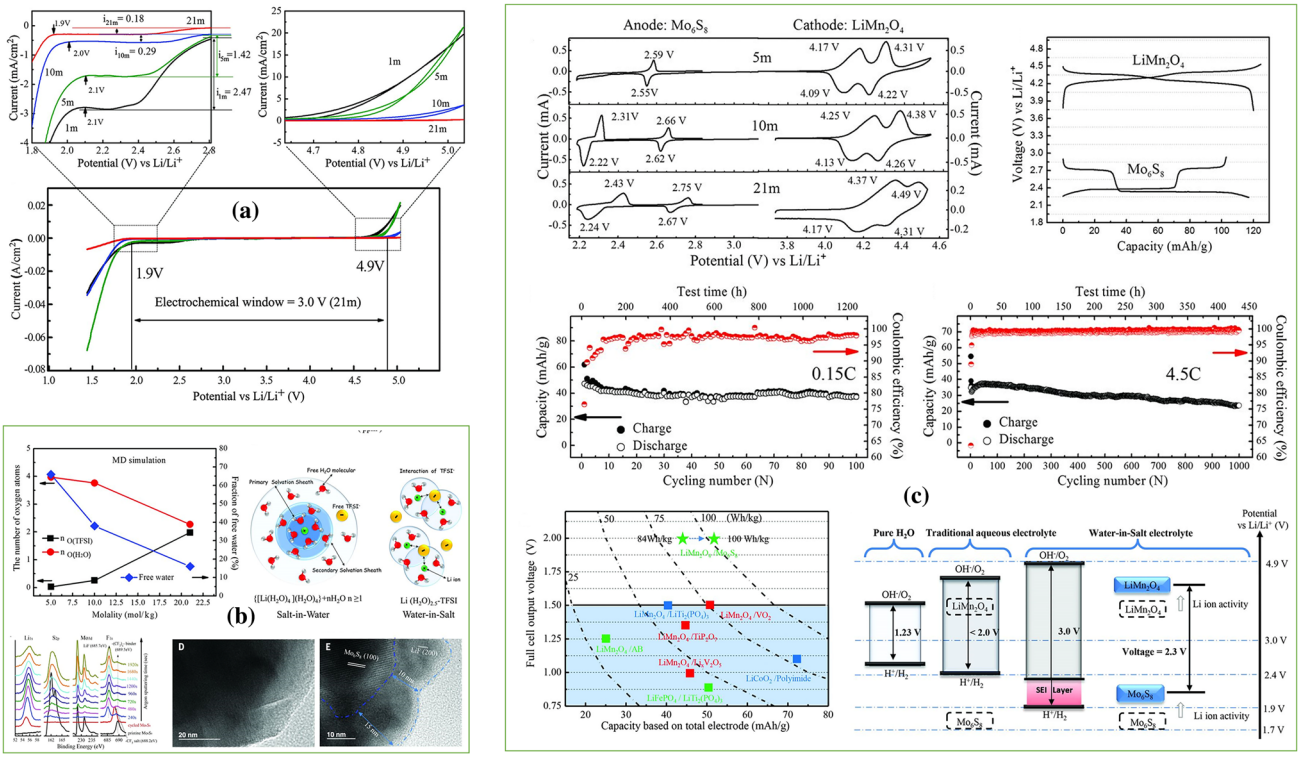

Figure 3. (a) The electrochemical window of LiTFSI-H_2O electrolytes. (b) The effect of LiTFSI concentration in aqueous electrolyte. (c) The electrochemical performance on active electrodes and ALIB based on the proposed aqueous electrolytes.[35] Adapted from Ref [35].

Activated carbon (AC) is a stable electrode material, which has been widely applied in aqueous electrolyte-based energy storage system. The mechanism of electrochemical double-layer capacitance is adsorption/desorption reactions of lithium ions on the surface of AC electrodes. A hybrid ALIB has been constructed by our group, which is composed of $LiMn_2O_4$ as the cathode material, AC as the anode material, and neutral Li_2SO_4 aqueous solution as the electrolyte.[36] In $LiMn_2O_4$ cathode, the Li^+ insertion/extraction is responsible for the electrode reaction, while the mechanism of electrode reaction is the Li^+ adsorption/desorption in AC anode. Between anode and cathode, Li^+ ion migration is the only ion transfer during the charge/discharge processes, which can be free from the issue involving the separation of anions and cations, such as the electrolyte consumption problem encountered in capacitors. The favorable reversibility is shown in the hybrid ALIB via optimizing the mass ratio of anode and cathode materials, the operating voltage window, and the pH value of electrolyte. A voltage range of 0.8–1.8 V is exhibited; meanwhile, a high energy density of 35 Wh kg^{-1} can be obtained together with the achievement of capacity retention of 95% (Fig. 4).[36] Besides $LiMn_2O_4$, the other intercalated cathode materials, such as $LiCoO_2$ and $LiCo_{1/3}Ni_{1/3}Mn_{1/3}O_2$, have also been developed, in which the corresponding electrochemical performance and decay mechanism have been investigated. Moreover, since the anions and cations are not separated during the operation of hybrid ALIBs, the gel electrolyte would be used instead of aqueous electrolyte.[31,37,38]

Aqueous Na-ion battery

Among various electrochemical ESSs, ASIBs show obvious advantages for sustainable energy due to the low cost (Fig. 5a). In the past decades, numerous efforts have been made to ameliorate the performance of ASIBs.[39–42] Albeit the mechanism of ASIBs is similar to that of conventional SIBs based on non-aqueous electrolytes, the electrochemical reactions of Na^+ insertion/extraction in aqueous electrolyte are more intricate, thereby making a profound impact on the development of electrode materials.[43–49] Figure 5b exhibits the relationship among hydrogen/oxygen evolution potentials, pH value, and the applied insertion/extraction potentials of Na ion.

Although ASIBs demonstrate great potential for grid-scale ESSs, the fundamental working conditions of ASIBs heavily depend on the intercalation of Na ion in aqueous electrolytes. Previous researchers have tried similar strategies to ALIBs that transition metal oxides are used as cathode materials, such as RuO_2 and MnO_2. Whereas, the abovementioned metal oxide cathode materials typically exhibit capacitance behavior, that is, the Faraday adsorption/desorption processes occur on their surface instead of Na-ion insertion/extraction reactions.[50,51] In the subsequent years, Whitacre's group have proposed $Na_{0.44}MnO_2$ (NMO) with a tunnel structural material as cathode, which displays three redox potentials (− 0.3 V to 3 V vs Hg/Hg_2SO_4) in Na_2SO_4 aqueous electrolyte and reveals the process of multiphase behavior during the Na^+ insertion/extraction processes.[52] Driven by the limited capacity of $Na_{0.44}MnO_2$, Wang's

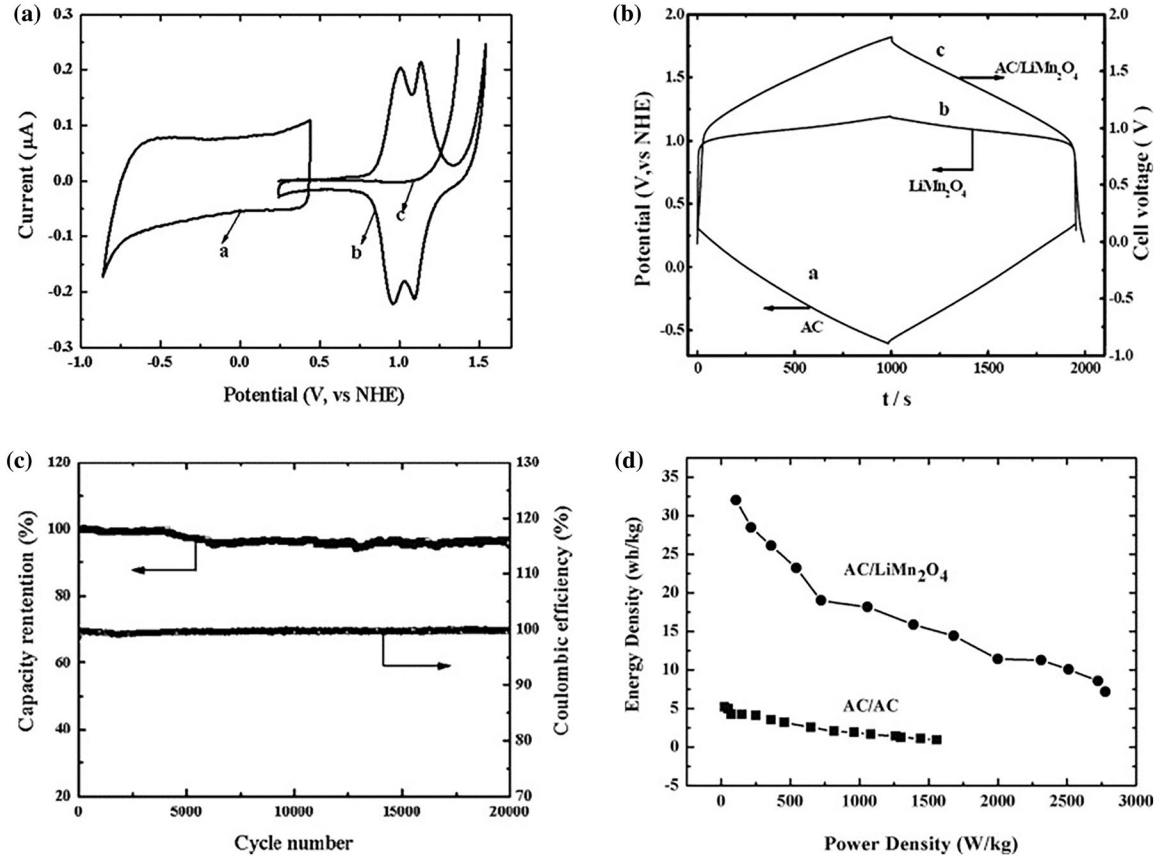

Figure 4. (a) The CV curves of AC, $LiMn_2O_4$, and carbon black. (b) The typical charge/discharge curves of AC, $LiMn_2O_4$, and hybrid aqueous AC/$LiMn_2O_4$ cell. (c) The cycle life of AC/$LiMn_2O_4$ cell. (d) Ragone plots of hybrid cell based on AC/1 M Li_2SO_4/$LiMn_2O_4$ and EDLC assembled by AC/1 M Li_2SO_4/AC.[36] Adapted from Ref [36].

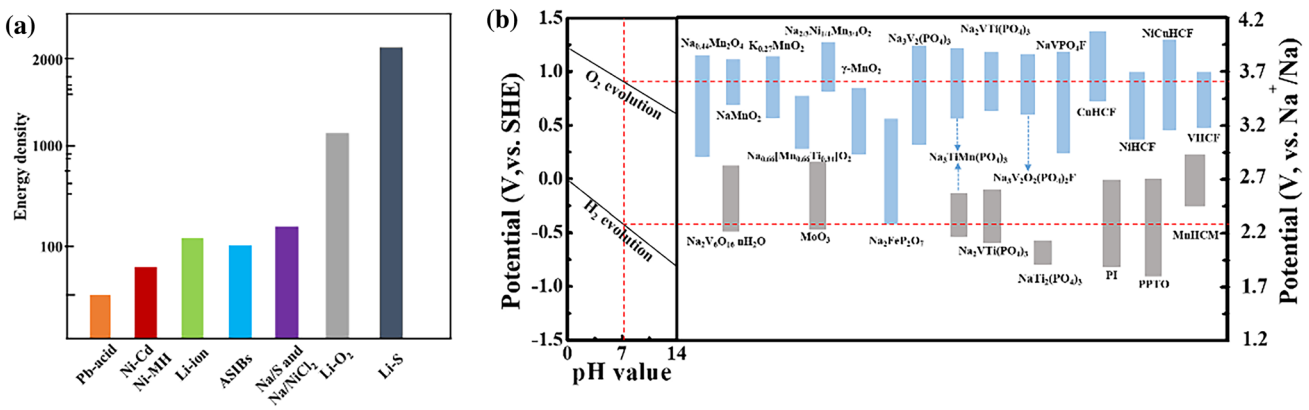

Figure 5. (a) The comparison on the energy density among various energy storage systems. (b) The electrochemical stability window of aqueous electrolyte under different pH values and the redox potentials of electrode materials for ASIBs.[42] Adapted from Ref [42].

group have reported a novel Na-rich tunnel-type cathode materials $Na_{0.66}[Mn_{0.66}Ti_{0.34}]O_2$ and $Na_{0.44}[Mn_{0.66}Ti_{0.34}]O_2$.[53] In addition, Kim and co-workers have investigated the electrochemical characteristics of Na-ion intercalation in 1 M Na_2SO_4 electrolyte among $Na_{2.7}Ru_4O_9$ and $Na_{0.44}MnO_2$, which present the similar structures. The $Na_{2.7}Ru_4O_9$ cathode exhibits three redox peaks during the first cycle with a capacity of 28 mAh g^{-1}.[54]

"Polyanionic" compounds deliver stable open framework and strong inductive effect of the anions, which are considered as a kind of ideal cathode material with desirable performance,

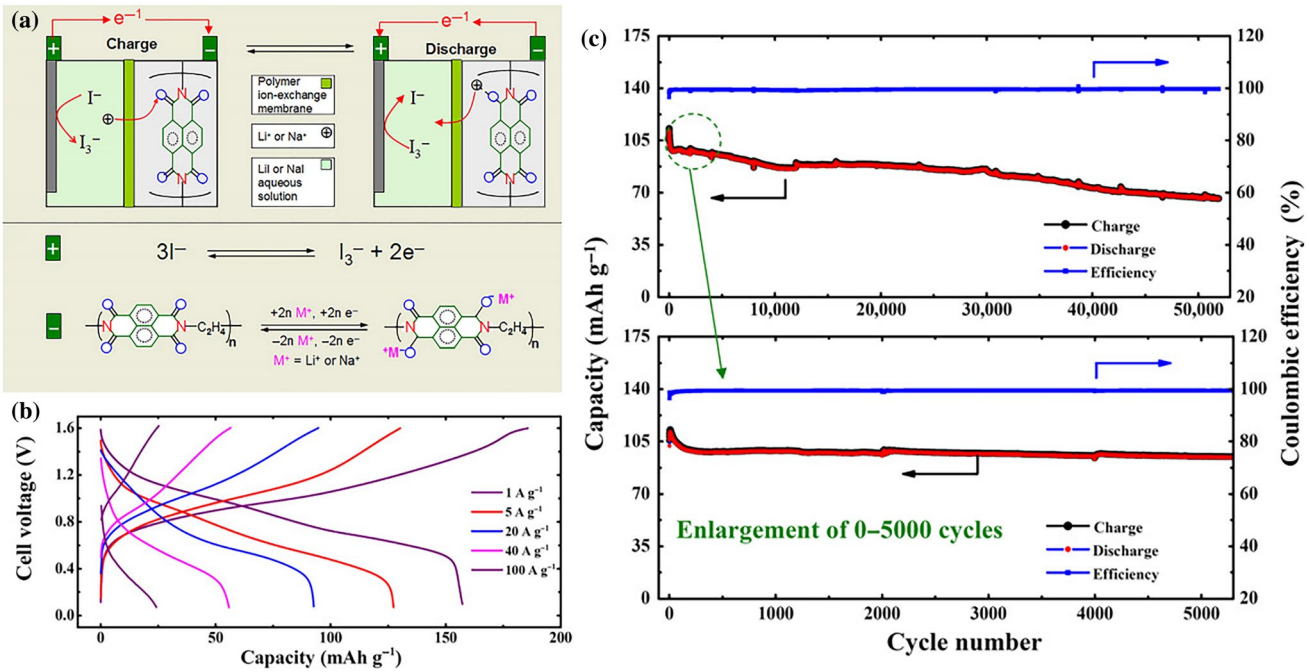

Figure 6. (a) Schematic illustration of the cell structure together with the corresponding electrode reactions. (b) The charge/discharge curves of ASIB based on liquid I^-/I_3^- cathode. (c) Long cycle life of the proposed ASIB. Reproduced with permission.[69] Adapted from Ref [69].

including long cycle life, improved rate capability, and favorable safety.[55–59] Inspired by the new phases of polyanionic compounds, $Na_4M_3(PO_4)_2P_2O_7$ (M = Fe, Mn, Co, and Ni) has been developed by Sanz et al., and subsequent researcher have further modified these materials for their utilization in non-aqueous sodium-ion batteries.[60,61] Besides the above phosphate-based materials, Kang and co-workers have reported a new material $Na_4Fe_3(PO_4)_2P_2O_7$, which shows two relatively low voltage plateaus (~ 2.9 and ~ 3.2 V vs Na^+/Na).[62] Nevertheless, the reversibility and cyclic stability of this material are not acceptable. The transition metals range from Fe to Ni, and Co and Mn increase the battery voltage from 3.2 V vs Na^+/Na to higher voltage for the $Na_4M_3(PO_4)_2P_2O_7$, which could cause the oxygen evolution in aqueous solution.[63] Therefore, further investigations are required to facilitate the future application of these high-voltage materials used as electrodes for ASIBs. Moreover, several polyanionic compounds have been found to show the promising application as cathode for ASIBs. A NASICON-type $Na_3V_2(PO_4)_3$ (NVP) cathode with broad tunnels have been developed to adapt the large Na ion and achieve the intercalation/de-intercalation processes with the absence of lattice perturbation, which shows the favorable electrochemical activity in various aqueous electrolytes.[58,64]

Apart from the aforementioned materials, Prussian blue analogs (PBAs) are another significant type of cathode material for ASIBs because of the favorable properties. Firstly, the open framework crystal structures of PBAs show wide interval space, which facilitates to achieve the rapid insertion/extraction reactions for alkali metal ion. Recently, a new type of PBAs composed of vanadium and iron ions (V/Fe PBAs) has been proposed as a cathode material for ASIBs.[65] Benefited from the multielectron redox reactions of V and Fe ions, the improved discharge capacity (90 mAh g^{-1}) has been obtained for V/Fe PBAs compared to previous reported Cu/Fe and Ni/Fe PBAs. However, the PBAs would transfer from the insoluble state to the soluble state due to the Fe-ion solubility by the water attack.[66] Finally, the PBAs would transform to the fully reduced state after cycling. To solve the problem, it is a promising strategy to apply the highly concentrated aqueous electrolytes, reducing the reaction activity of water and improving the PBAs stability.[67] Besides the above-mentioned cathode materials, large efforts have been made to develop different compounds as cathode materials for ASIBs. For example, the $NaMn_{1/3}Ni_{1/3}Co_{1/3}PO_4$ maricite has been used as cathode material in aqueous NaOH electrolyte to develop stationary renewable energy storage applications, in which AC is used as anode.[68] Recently, our group has developed a new aqueous battery system, which is based on the redox of I^-/I^{3-} couple in liquid cathode together with the reversible enolization in polyimide anode. Subsequently, through employing a Na^+/Li^+ exchange polymer membrane, Na^+ (or Li^+) transfers between the above cathode and anode.[69] As depicted in Fig. 6a, the I^{3-} ions can be obtained through the oxidation of I^- ions during the charge process. At the same time, Na ion (or Li ion) in the liquid cathode shuttle through the ion exchange membrane and react with the polyimide anode to produce Na*x*–polyimide (or Li*x*–polyimide) via an "enolization process." Figure 6b demonstrates the rate capability of the aqueous Na-ion battery, which has achieved a favorable capacity of 95 mAh g^{-1} at a high current density (20 A g^{-1}) and retained a satisfactory capacity of 28 mAh g^{-1} even at a rather high current density (100 A g^{-1}). It is

unexpected that the full cell can achieve an ultra-long cycle (over 50,000 times), which is comparable to that of ALIB mentioned previously (Fig. 6c).

Albeit titanium-based materials have been intensively developed as anode materials for non-aqueous SIBs, only NASICON-type $NaTi_2(PO_4)_3$ has been reported as a promising anode candidate of ASIBs.[70–72] The reversible electrochemical Na-ion insertion/extraction into NASICON-type $NaTi_2(PO_4)_3$ for aqueous/non-aqueous SIBs have been first proposed by Park et al.[73] 2 mol of Na ion can be reversibly inserted/extracted in $NaTi_2(PO_4)_3$ on basis of Ti^{3+}/Ti^{4+} redox couple, leading to the achievement of a favorable reversible capacity of 133 mAh g^{-1}. Moreover, due to the low viscosity and fast ion migration of aqueous electrolyte, the $NaTi_2(PO_4)_3$ electrode displays lower electrochemical polarization in aqueous electrolyte than that in non-aqueous electrolyte. In order to fulfill the aggressive demand of efficient anode materials for ASIBs, a great deal of efforts have been focused on the exploration of other latent materials, like organic-based compounds. Although the organic electrode materials have been proposed from 30 years ago, numerous efforts are required to devote to facilitate the application of organic-based compounds in ASIBs.[74]

As a promising alternative to traditional organic Na-ion batteries, ASIBs are still confronted with several challenges, mainly including the evolution of H_2/O_2 from water, the reactions between electrode and water/oxygen jointly with proton co-insertion, and inevitable dissolution of active materials in aqueous electrolyte. To overcome the abovementioned shortcomings, the concentrated electrolytes could be utilized in ASIBs due to the inhibited water activity. As demonstrated by the obtained results, the high-concentration Li-ion electrolytes can play a critical role on broadening the electrochemical window and enhance the cycling stability of ALIBs.[35,75] Numerous research efforts have been imposed on investigating the effects of electrolyte concentration on the electrochemical performance of ASIBs. However, the selection of concentrated Na^+ aqueous electrolyte remains a challenge since a high-concentration Na_2SO_4 aqueous solution cannot be obtained due to its mild solubility. Additionally, the occurrence of corrosive side reactions has been reported in a $NaNO_3$ electrolyte with a high concentration of 5 M.[76] Moreover, even though the highly concentrated Na-bis(fluorosulfonyl)imide (NaFSI) electrolyte could accommodate electrochemical behaviors within a broad voltage window, there are still concerns about the stability of FSI^- anion in aqueous solution.[77] Therefore, the scientific and technical efforts in ASIBs are still required for their large-scale application.

Zinc anode-based batteries

Aqueous zinc-ion batteries (AZIBs) are expected as promising alternatives to lithium-ion batteries due to multiple merits of Zn anode including lower cost, resource abundance, nontoxicity and good compatibility with aqueous electrolyte.[78–86] Generally, an AZIB is assembled with a metallic Zn anode and a cathode (such as $Ni(OH)_2$, metal oxide, Br_2, and O_2) in aqueous electrolyte. However, Zn anode suffers from the issues, such as Zn dendrites, HER, and corrosion.[87,88] The Zn dendrite is derived from the uneven Zn plating. In the initial nucleation, the zinc ion is absorbed on Zn anode surface, nucleating on the location with the minimum surface energy. Subsequently, protrusion is formed, where zinc ion continuously accumulates to form the Zn dendrite. Moreover, the HER and corrosion exhibit the inseparable relationship. In the aqueous electrolyte, Zn and H_2O would spontaneously react with each other to produce H_2 due to the redox potential of Zn^{2+}/Zn (− 0.76 V vs. SHE). Meanwhile, high concentration of OH^- is generated to accelerate the corrosion, leading to the reaction between zinc ion and aqueous electrolyte. The corrosion reaction can be formulated as follows (Eq. 3):[89]

$$4Zn^{2+} + 6OH^- + {SO_4}^{2-} + xH_2O \leftrightarrow Zn_4SO_4(OH)_6 \cdot xH_2O. \quad (3)$$

The by-product would not protect the Zn anode, which is different from the SEI of Li anode. Recently, efforts have been devoted to solve these problems. The mechanical shielding for Zn anode shows promising to suppress the Zn dendrite via strengthening the surface coating and separator.[90] The surface coating is to construct a protective layer on the anode surface, which can provide the physical protection for Zn anode. The main purpose is to improve the Zn plating behavior, which can be obtained via restraining the migration path of Zn ions, providing the even electric field and nucleation site. Besides regulating the transfer of zinc ion, a multifunctional separator can be designed to interact with zinc ion, which exhibits the zincophilicity to induce the even Zn plating. Moreover, modifying the electrolyte, such as employing the electrolyte additive and solid-state electrolyte, would effectively inhibit the side reactions of hydrogen evolution and corrosion. In the following section, zinc anode-based batteries will be discussed in detailed, and the corresponding perspectives will be provided as well.

Zn-metal oxide battery

The typical cathode materials of AZIBs are manganese dioxides and vanadium oxides, whose price is much lower than that of traditional cathodes ($LiCoO_2$, $LiMn_2O_4$, and $LiFePO_4$) in current lithium-ion batteries. Therefore, AZIBs with low cost and appropriate energy densities exhibit great potential as large-scale ESSs in the commercial application. The reaction mechanism of metallic Zn anode is based on the reversible platting/stripping process. By contrast, the structure and reaction mechanism of metal oxides cathode in AZIBs are complicated. In this part, we focus on typical cathode materials, including manganese dioxides and vanadium-based oxides. According to the distinct structural features, MnO_2 cathodes in AZIBs are usually classified into three categories: (1) tunnel-type (α-MnO_2, β-MnO_2, and γ-MnO_2), (2) layered-type (δ-MnO_2), and (3) spinel-type $ZnMn_2O_4$. It is noteworthy that the possibility of structure transformation into another type during chemical/electrochemical processes could affect the electrochemical performance of MnO_2 cathodes. Among these polymorphs, layered-type MnO_2 cathode has attracted intense

research interest owing to its large interlayer spacing favorable to rapid Zn^{2+} diffusion kinetics.

The electrochemical mechanisms for MnO_2 cathodes are still controversial in different cases varying with structure categories, morphologies, fabrication procedures, and operating conditions. Even though, the main reaction mechanisms can be summarized as below:

(1) Zn^{2+} insertion/extraction mechanism. For example, α-MnO_2 cathode has been reported to operate according to Eq. (4).

$$Zn^{2+} + 2e^- + 2MnO_2 \leftrightarrow ZnMn_2O_4. \quad (4)$$

(2) H^+/Zn^{2+} co-insertion/extraction mechanism. Accompanied with the Zn^{2+} insertion and the formation of $ZnMn_2O_4$ products, simultaneous H^+ insertion process results in the formation of MnOOH products at the discharged state.

(3) Conversion reaction mechanism. Since MnO_2 reacts with H^+ derived from water to generate MnOOH, the remaining OH^- can react with the zinc salt in the electrolyte to form the deposits on the electrode surface. Therefore, the conversion reaction between MnO_2 and MnOOH is accompanied with reversible formation/decomposition of zinc hydroxide sulfate species, which can be represented as the following reactions (Eqs. 5 and 6).

$$H_2O \leftrightarrow H^+ + OH^- \quad (5)$$

$$MnO_2 + H^+ + e^- \leftrightarrow MnOOH. \quad (6)$$

Vanadium-based oxides are appealing to be cathode candidates due to their high specific capacities stemming from the multiple valences of vanadium (V^{2+}, V^{3+}, V^{4+}, and V^{5+}). Through linking structural units of V–O polyhedrons (such as VO_4 tetrahedron, VO_5 square pyramid, and VO_6 octahedron), the distinct framework structures of vanadium oxides are assembled. Notably, the pre-intercalated cations (H^+, Li^+, Na^+, K^+, NH_4^+, Ag^+, Mg^{2+}, Ca^{2+}, Ba^{2+}, Zn^{2+}, Al^{3+}, etc.) or water molecules could enhance the structural stability of vanadium-based oxides, affecting the electrochemical behaviors of AZIBs. Vanadium-based oxides can be divided into three categories as follows: (1) V_2O_5 and $M_xV_2O_5$ (M is metal ions) composed of single/double lattice layers of VO_5 square pyramids and VO_6 octahedrons, (2) layered $M_xV_3O_8$ (M is NH_4^+ or H^+ or alkali cation) composed of corner-sharing VO_5 square pyramids and VO_6 octahedrons, and (3) tunnel-type vanadium-based oxides with a three-dimensional framework, such as VO_2, V_6O_{13}, $Zn_xV_2O_7$, and $K_2V_8O_{21}$. The electrochemical mechanisms of vanadium oxides cathode mainly include (1) Zn^{2+} insertion/extraction mechanism, (2) Zn^{2+}/H^+ co-insertion mechanism, and (3) Zn^{2+}/H_2O co-insertion mechanism.

(1) Zn^{2+} insertion/extraction mechanism. Vanadium-based oxides with a layered or tunnel-type structure provide large space to accommodate Zn^{2+}, and Zn^{2+} insertion/extraction is accompanied with the variation of vanadium valence state. In addition to the slower diffusion-controlled behaviors, pseudocapacitance behaviors with rapid charge transfer kinetics could also contribute to decent high-rate performance of AZIBs with vanadium-based cathode.

(2) Zn^{2+}/H^+ co-insertion mechanism. Different from the abovementioned H^+/Zn^{2+} co-insertion behaviors in MnO_2 cathode, H^+/Zn^{2+} co-insertion mechanism in vanadium-based oxides is more complicated. The sequence of H^+/Zn^{2+} insertion/extraction (two-step or simultaneous), the pseudocapacitance contribution of H^+, the position of the inserted H^+, and the influence of H^+ insertion/extraction on the electrolyte and the anode are still unclear.

(3) Zn^{2+}/H_2O co-insertion mechanism. Owing to the pre-intercalated cations or water molecules, vanadium-based oxides with enlarged interlayer space are usually favorable for hydrated Zn^{2+} insertion. Actually, the solvating H_2O molecules can shield partial charge of divalent Zn^{2+} cations and decrease the electrostatic attraction between guest Zn^{2+} and the lattice oxygen. Therefore, the co-insertion of solvating H_2O as a "lubricant" is conductive to fast Zn^{2+} diffusion within the electrode.

The specific capacities of metal oxide cathodes (generally <400 mAh g^{-1}) based on the Zn^{2+} insertion/extraction mechanism are highly inferior to that of Zn anode (860 mAh g^{-1}), which limits the development of AZIBs with high energy densities. Another tricky issue for typical cathode materials is rapid capacity declining, which is caused by their irreversible structural conversion and inevitable dissolution in aqueous electrolyte upon cycles. Furthermore, the poor intrinsic electronic conductivity of metal oxides and the desolvation process at the electrode/electrolyte interface will slow the charge transfer kinetics, which would be detrimental to the rate performance of AZIBs. On the other hand, the specific capacities of AZIBs are also restricted by low utilization rate of Zn anode, which results from a combination of numerous issues, such as low-efficiency Zn plating/stripping behaviors, surface passivation, hydrogen evolution reaction, and dendrite growth. Additionally, a narrow electrochemical stability window of aqueous electrolytes could affect the Zn plating/stripping behaviors, and the side reaction of H_2/O_2 evolution should be carefully considered with the employment of aqueous electrolyte.

In order to alleviate the capacity fading of manganese dioxide cathodes caused by phase conversion, a guest polymer can be pre-intercalated into the interlayer space of MnO_2 cathode to enhance the stability of structure. A polyaniline (PANI)-intercalated MnO_2 with the significantly improved electrochemical performance for AZIB is developed, as shown in Fig. 7a. A H^+/Zn^{2+} co-insertion mechanism is found during discharging (Fig. 7b). At the initial stage of discharging, H^+ insertion is more competitive than Zn^{2+} insertion, leading to the increase of OH^- concentration. At the second discharge platform, Zn^{2+} insertion is dominant and zinc hydroxide sulfate is formed, as illustrated in Fig. 7c. Owing to this durable reaction mechanism and the "pillar" effect of intercalating PANI guest, the AZIB delivers a high specific capacity of 280 mAh g^{-1} without obvious capacity fading upon 200 cycles at a current of 200 mA g^{-1} (Fig. 7d).[91]

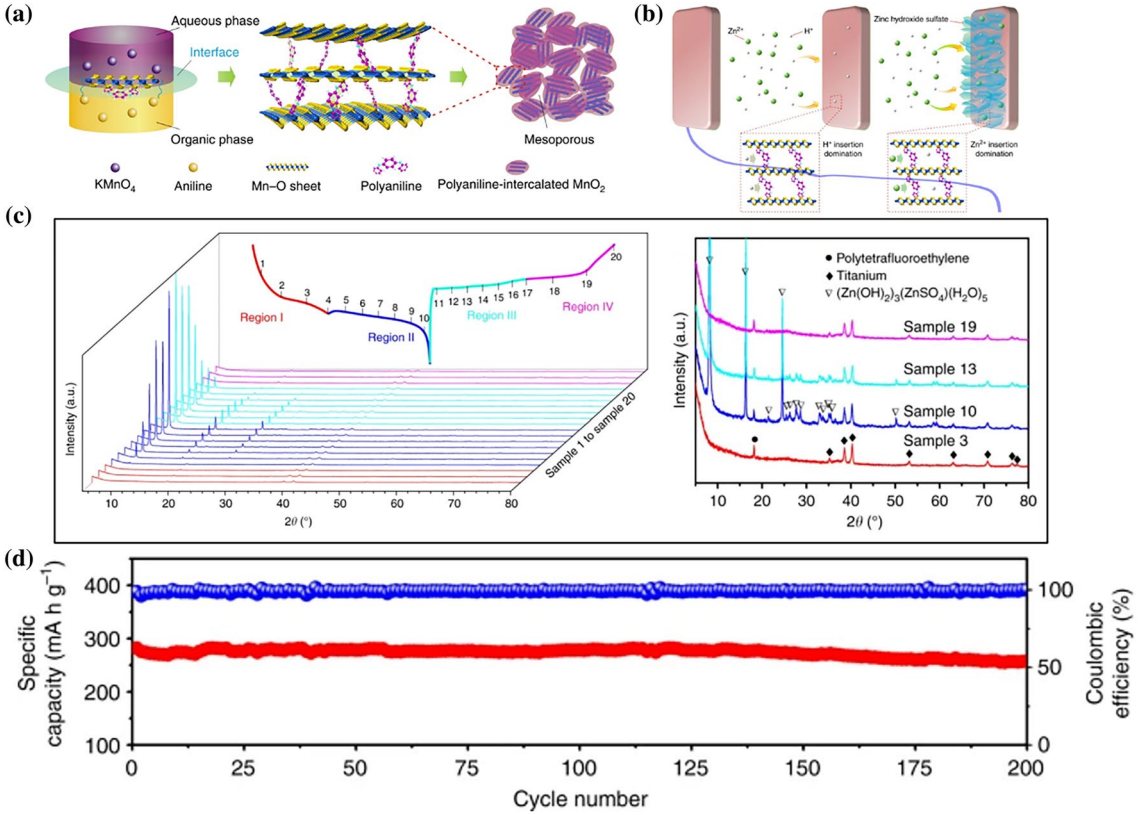

Figure 7. (a) Schematic preparation of the PANI-intercalated MnO_2 cathode. (b) Schematic diagram of the H^+ and Zn^{2+} co-insertion mechanism. (c) Evolution of ex situ XRD patterns of the cathode during cycling. (d) The cycle performance at 200 mA g^{-1}.[91] Adapted from Ref [91].

Similarly, introducing a conductive polymer into the interlayer space of vanadium-based cathodes is a feasible strategy to facilitate the electronic conductivity and strengthen the layer structure.[92] Our group has employed poly(3,4-ethylenedioxythiophene) (PEDOT) to intercalate into ammonium vanadate oxide (NVO), which can enlarge the interlayer space of NVO and avoid the capacity fading from structural degradation (Fig. 8a). As demonstrated by the ex situ XRD patterns in Fig. 8b, the reaction mechanisms can be formulated as follows: $PEDOT/NH_4V_3O_8 + x Zn^{2+} + 2xe^- \rightarrow PEDOT/Zn_xNH_4V_3O_8$ at the initial discharge process and $PEDOT/Zn_xNH_4V_3O_8 - y Zn^{2+} - 2ye^- \rightarrow PEDOT/Zn_{x-y}NH_4V_3O_8$ at the following charging process. Due to the magnified interplanar spacing of the NVO crystal lattice and the improved electronic conductivity of conductive polymer, the PEDOT-intercalated NVO cathode exhibits superior rate capability compared to bare NVO (Fig. 8c). Additionally, an ultra-high capacity retention rate of 94.1% is maintained after 5000 cycles at 10 A g^{-1} resulting from the robust layer structure during repeated cycles.[93]

Zn-air battery

Zinc-air batteries provide appealing solutions to the next-generation ESSs due to the inherent properties of high safety, environmental friendliness, and potential low cost.[94–98] Zinc-air batteries show a high specific energy density (1218 Wh kg^{-1}) and volumetric energy density (6136 Wh L^{-1}), which present the promising application.[99] During discharging, O_2 diffuses into the air electrode and then it is reduced to hydroxide ions through the oxygen reduction reaction (ORR), which can be formulated as follows: $O_2 + H_2O + 4e^- \leftrightarrow 4OH^-$.[100] A high voltage of 1.66 V can be produced; however, ORR is kinetically slow.[101] To enhance the energy efficiency of zinc-air batteries, an efficient strategy is provided to design a bifunctional electrocatalyst for ORR and OER. Pt, IrO_2, and RuO_2 serve as the traditional electrocatalysts for ORR and OER, while the high cost and insufficient stability restrain the further application. Instead of the noble metal electrocatalyst, the combination of heteroatom-doped carbon and transition metal oxides delivers decent ORR and OER activity.[97] N-doped carbon nanomaterials have been widely applied in electrocatalyst, which show favorable electronic properties and surface polarities. Thus, the combination with N-doped carbon nanomaterials is a promising strategy to prepare bifunctional electrocatalyst.[98] Wang's group has reported an electrocatalyst composed of Co nanoparticles wrapped with nitrogen-doped graphene, as shown in Fig. 9a.[102] The graphene-supermolecule complexes exhibit a decent catalytic performance for ORR/OER.

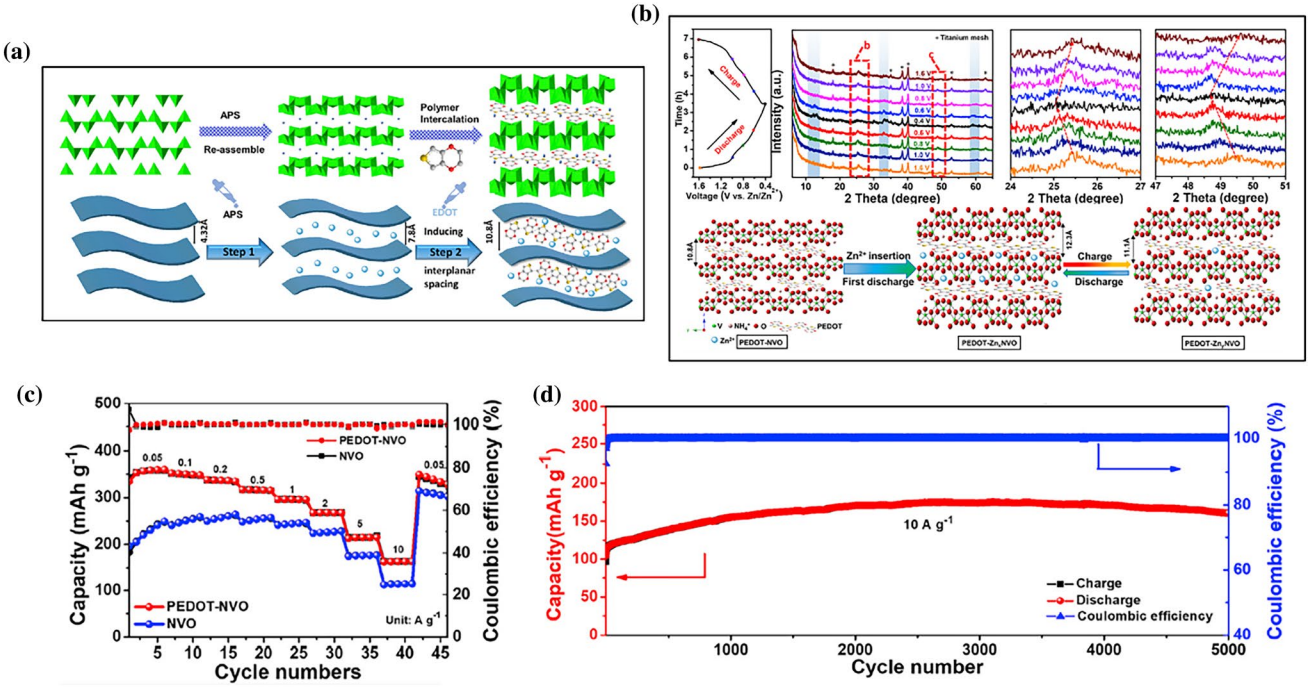

Figure 8. (a) Schematic formation of the PEDOT-intercalated NVO cathode. (b) Ex situ XRD patterns and schematic Zn^{2+} intercalation of the PEDOT-intercalated NVO cathode during discharge and charge processes. Electrochemical performance of PEDOT-intercalated NVO cathode: (c) rate capability and (d) cycling performance at 10 A g^{-1}.[93] Adapted from Ref [93].

Compared to Pt catalyst, the electrocatalyst shows positive onset potential (0.943 V) together with half-wave potential (0.864 V) due to the abundant carbon defects accelerating reaction rate, as displayed in Fig. 9b. A four-electron process is indicated in Fig. 9c which shows that the electron transfer number is 3.97. Moreover, a long-term cycle life of 667 h and peak power density of 205 mW cm^{-2} are delivered in Fig. 9d, which benefit from the M-N_x and defective N-doped C improving ORR and OER activity. Thus, it can be found that the transition metal–nitrogen–carbon materials are appealing candidates on account of their rich active sites and decent electronic structures. Our group has developed an ordered macroporous carbon catalyst with interconnected structure for zinc-air battery in Fig. 10a.[103] The interconnected macroporous can be obviously observed by the transmission electron microscopy (TEM) in Fig. 10b, which clearly shows the macropore diameter of 350 nm. The bifunctional electrocatalyst provides abundant cobalt-nitrogen-carbon active sites, which can enhance the ORR and OER activity. During the battery operating, the cobalt and nitrogen species are positively involved in the ORR/OER active sites. Charge can be induced to transfer from N to neighboring C atoms due to the weakened O–O bond derived from nitrogen species, and subsequently, oxygen electrocatalysis is facilitated. Therefore, a high power density of 221.1 mW cm^{-2} is shown in Fig. 10c as well as a cycle life of 160 h exhibiting 5 mA cm^{-2} is shown in Fig. 10d. The voltage gap of electrocatalyst shows only a slight increasing. Although commercial primary alkaline zinc-air batteries have been successfully applied, they are still limited by the issues associated with Zn dendrite growth, HER corrosion, sluggish kinetics, etc. Wang's group has developed a non-alkaline rechargeable zinc-air battery to reduce these issues.[104] Zinc trifluoromethanesulfonate ($Zn(OTF)_2$) aqueous solution is employed as the electrolyte, which could establish H_2O-poor and Zn^{2+}-rich structure at the cathode surface (Fig. 11a). The OTF^- anion is hydrophobic, which shows weak interaction with Zn^{2+} ion. This can bring in $2e^-$ ORR chemistry and the highly reversible ZnO_2 can be produced, as observed in Fig. 11b and c. In the highly hydrophilic $ZnSO_4$ aqueous solution, OH^- is generated during ORR process, in which the reversibility of hydrated products $Zn_4(OH)_6SO_4{\cdot}0.5H_2O$ (ZHS) is limited. Moreover, a $3.79e^-/O_2$ is also detected in $ZnSO_4$ aqueous electrolyte (Fig. 11d). During ORR process, a $1.97e^-$ transfer per O_2 molecule (e^-/O_2) is detected in $Zn(OTF)_2$ aqueous solution (Fig. 11e). Compared with alkaline and $ZnSO_4$ electrolyte, the zinc-air battery based on $Zn(OTF)_2$ aqueous electrolyte shows high electrochemical performance and the limited side reactions. Thus, a long cycle life of 1600 h and 160 h is obtained in ambient environment at 0.1 mA cm^{-2} and 1 mA cm^{-2}, respectively (Fig. 11f). Moreover, a high specific capacity of 684 mAh g^{-1} can be delivered as well as a utilization efficiency of 83.1% can be obtained (Fig. 11g). For rechargeable Zinc-air batteries, air electrodes are responsible for both efficient ORR and OER through using the bifunctional electrocatalysts.[105] However, the cycle stability of bifunctional electrocatalysts is usually poor. Further researches are required to devote to promote the

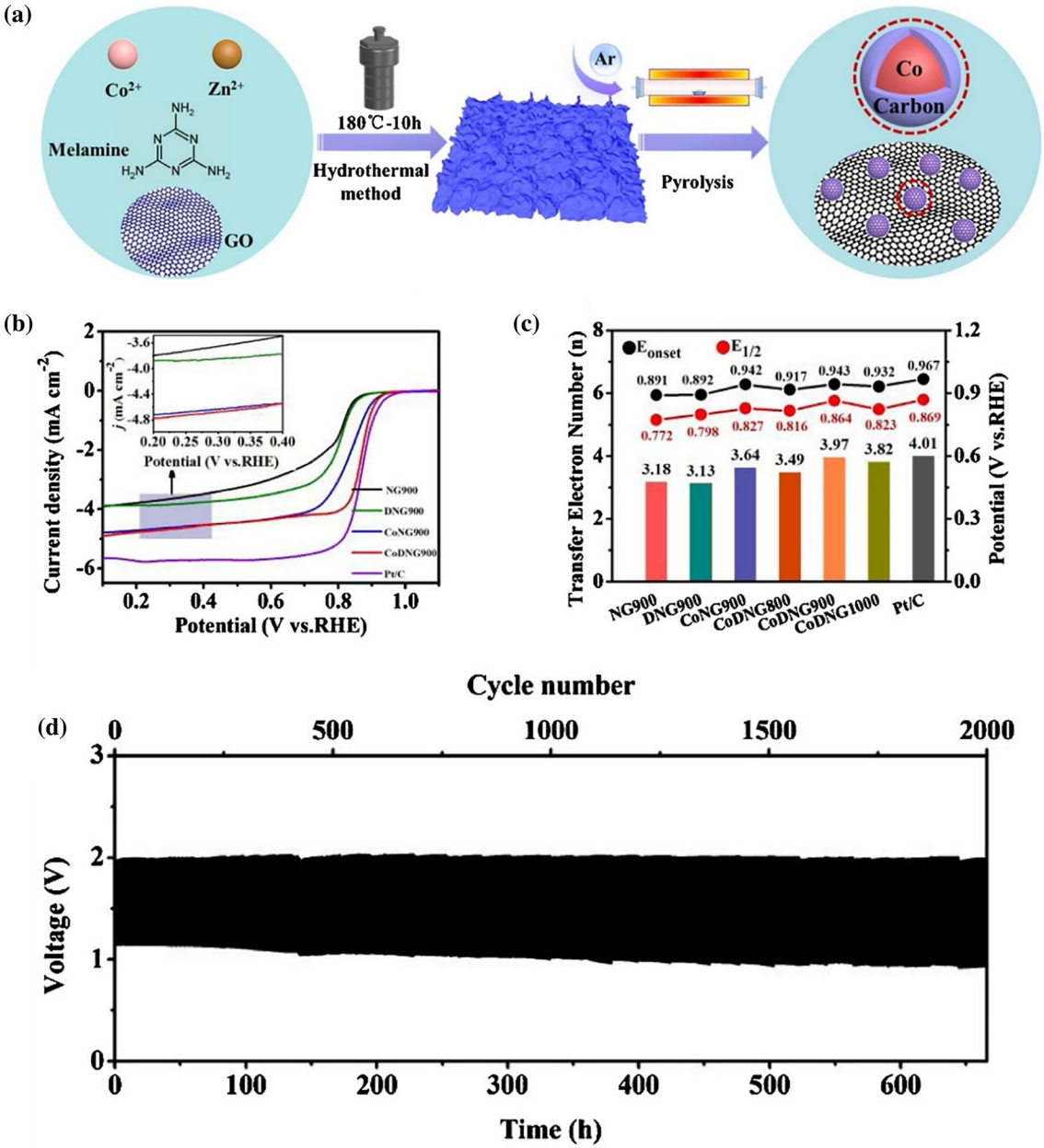

Figure 9. (a) Schematic preparation of electrocatalyst. (b) ORR LSV curves for the electrodes. (c) $E_{1/2}$, E_{onset}, and n for the various catalysts. (d) Charge/discharge curves for the Zn-air battery at 10 mA cm^{-2}.[102] Adapted from Ref [102].

development of rechargeable zinc-air batteries through developing the efficient and stable bifunctional electrocatalysts.[106] Except for the electrocatalysts, alkaline electrolyte is generally introduced to the rechargeable zinc-air batteries, which still beset the practical application.[107] It has been demonstrated that the favorable electrochemical performance is exhibited in mild acidic aqueous electrolyte. Therefore, the mild acidic or neutral electrolytes could also be the promising candidates for the rechargeable aqueous zinc-air batteries.

Zn–Br_2 battery

The zinc/bromine system can date back to 1885, which would be the oldest rechargeable flow battery (RFB) hybrid system. A typical Zn–Br_2 flow battery consists of two reservoirs for $ZnBr_2$ electrolyte storage, the reactor, as well as connecting pipes and pumps. The electrochemical behaviors in Zn–Br_2 battery are based on the following redox reactions (Eqs. 7 to 9):

$$\text{Cathode: } 2Br^- \leftrightarrow Br_2 + 2e^- \quad \left(E^0 = 1.08 \text{ V vs. SHE}\right) \quad (7)$$

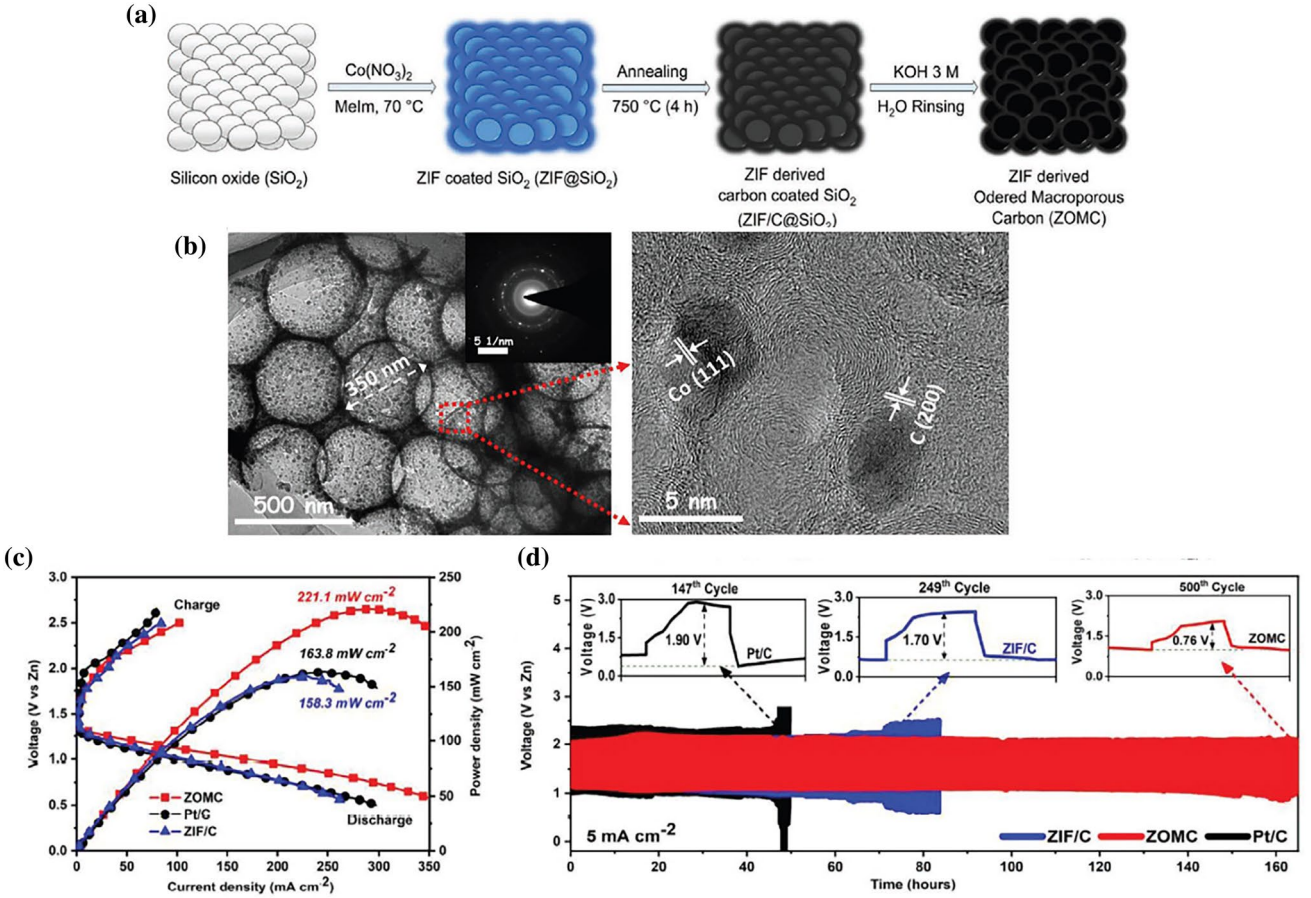

Figure 10. (a) Schematic synthesis process of electrocatalyst. (b) TEM and HRTEM images of the electrocatalyst. (c) The discharge/charge polarization curves and power density plots. (d) Cycling tests at 5 mA cm^{-2} for the different zinc-air batteries.[103] Adapted from Ref [103].

$$\text{Anode: } Zn^{2+} + 2e^- \leftrightarrow Zn \quad \left(E^0 = -0.76 \text{ V vs. SHE}\right) \quad (8)$$

$$\text{Overall: } Zn^{2+} + 2Br^- \leftrightarrow Br_2 + Zn \quad \left(E^0 = 1.84 \text{ V}\right). \quad (9)$$

Br_2 is obtained at the cathode during charge process. Despite a low solubility of bromine in water (0.43 mol L^{-1} at 20 °C), highly soluble polybromide (Br_3^-) can be generated due to the existence of bromide ions, while the deposition of metallic Zn occurs at the anode (generally carbon anode) simultaneously. Reversely, Br_2 is reduced to Br^- at the cathode accompanying with zinc dissolution at the anode during discharge, which can deliver a high theoretical energy density (432 Wh kg^{-1}). Generally, to inhibit dendrite growth at the anode and the consequent battery failure, a spacer component is required to ensure adequate space for Zn deposition between electrode and membrane. In order to avoid base-assisted bromine hydrolysis in aqueous solution, strongly acidic electrolytes containing halides and complexing agents are selected for Zn–Br_2 RFBs to ensure favorable bromine conservation, in which the charging products Br_2 is in equilibrium with Br_3^-. Although highly soluble Br_3^- can boost reaction kinetics, the diffusion of Br_3^- species through the membrane arouses detrimental reaction between Br_3^- and metallic Zn. Subsequently, it would lead to low coulombic efficiency together with high self-discharge current. Due to the competition of electrode corrosion reaction involving flowable Br_2/Br_3^- species with intrinsic redox reaction, the reversibility of electrochemical behaviors is deteriorated, ultimately leading to battery failure. Additionally, the formation of zinc dendrites is a common issue for zinc-based battery, which could give rise up to an internal short circuit. Furthermore, a low power density and operating current density caused by severe electrochemical polarization would seriously limit the development of Zn–Br_2 RFBs.

To overcome these shortcomings, multiple strategies have been proposed for Zn–Br_2 RFBs. The diffusion of soluble Br_3^- species could be restricted through the introduction of complexing agents or organic solvents. Particularly, the interaction between polybromide species and large asymmetric quaternary ammonium cations is able to form a hydrophobic organic phase, which leads to the separation of polybromide complexes from the aqueous electrolyte. The utilization of ion-selective membranes is another efficient approach to hinder cross-membrane diffusion and consequently eliminate the corrosion

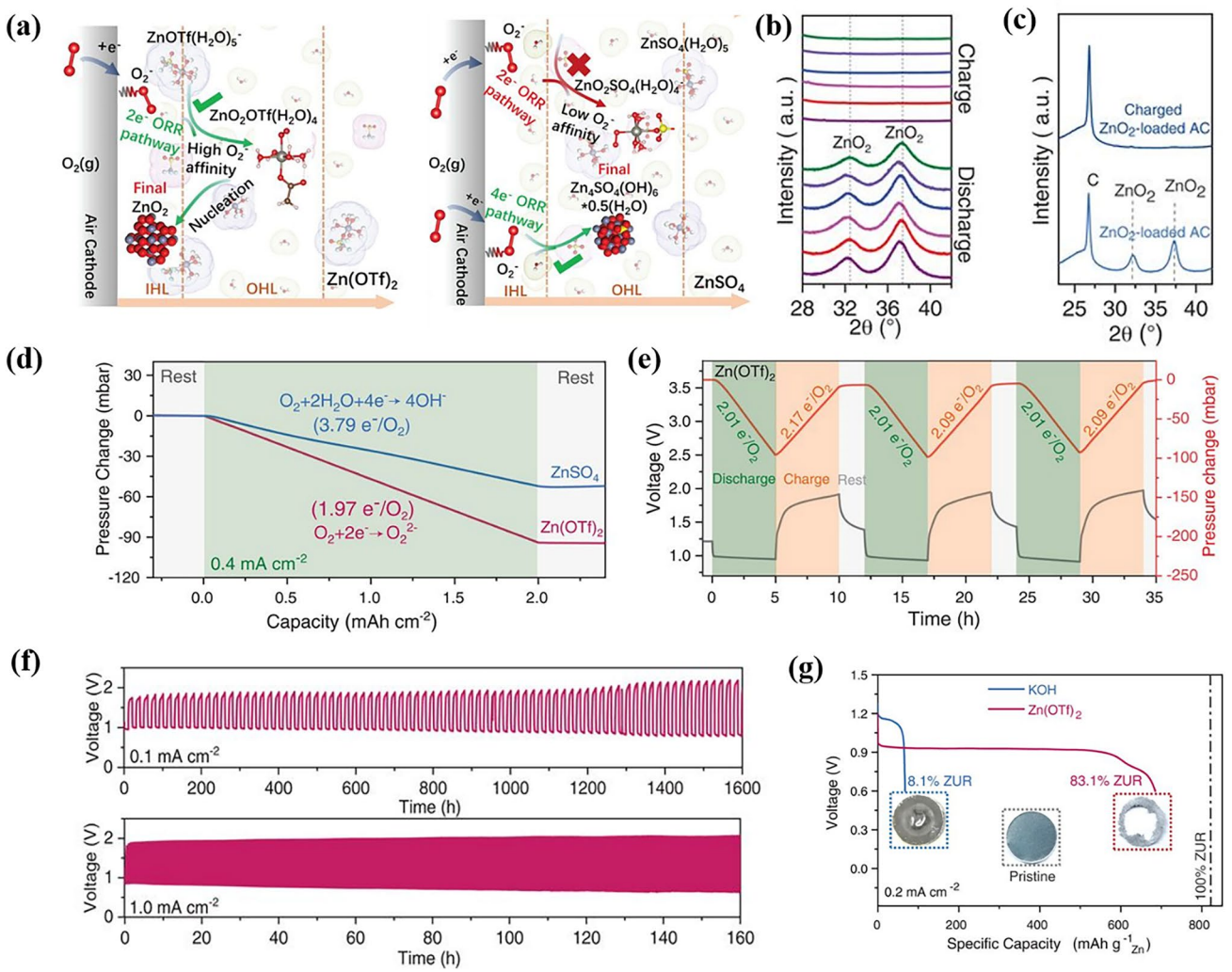

Figure 11. (a) Schematic reaction processes in the inner and outer Helmholtz layer at the surface of air electrodes using $Zn(OTf)_2$ and $ZnSO_4$ electrolytes, respectively. (b) XRD patterns of ZnO_2. (c) XRD patterns of the ZnO_2-loaded air cathodes before and after charge. Evolution of the Zn–O_2 battery mechanism at various electrolytes during a discharge process: (d) pressure change in the gas reservoir under neat O_2 atmosphere and (e) pressure change during galvanostatic discharge and charge at 0.4 mA cm^{-2}. (f) Cycle performance of the Zn-air batteries at 0.1 and 1.0 mA cm^{-2}, respectively. (g) Galvanostatic discharge profiles of the zinc-air batteries in different electrolytes.[104] Adapted from Ref [104].

of zinc anode by Br_3^-, which could alleviate self-discharge and short circuit at zinc anode. For the purpose of enhancing the power density of Zn–Br_2 RFBs, highly active electrode materials are designed in pursuit of rapid Br_2/Br^- redox behaviors. A self-supporting 3D hierarchical composite has been prepared via in situ growth method as the electrode in Zn–Br_2 flow battery (Fig. 12).[108] The electrochemical polarization is significantly alleviated owing to multiple merits of this composite electrode, including TiN nanorods endowing the favorable catalytic activity for Br_2/Br^- redox reaction, and a carbon felt ensuring a 3D electron conductive network. In addition, the ionic transport kinetics has been significantly facilitated resulting from the improved electrolyte penetration into the 3D hierarchical nanorod array structure. As a result, the operating current density of a zinc–bromine flow battery based on this proposed composite electrode has been risen to 160 mA cm^{-2}, which is superior to most reported results.[109] The transformation from a flow battery system into a static energy storage system would offer a fundamental solution to cross-diffusion and self-discharge problems for Zn–Br_2 battery techniques. Liang's group has reported a zinc–bromine static battery utilizing glass fiber separator without these auxiliary parts, like pumps, connecting pipes, and reservoirs as well as ion-selective membranes (Fig. 13).[109] Through the introduction of a multifunctional additive, tetrapropylammonium bromide (TPABr), flowable bromine has been transformed into a dense solid state, effectively restraining the cross-diffusion of bromine species and the growth of zinc dendrites. Therefore, this Zn–Br_2 static battery shows an excellent electrochemical performance, including a high energy density of 142 Wh kg^{-1} with the energy efficiency

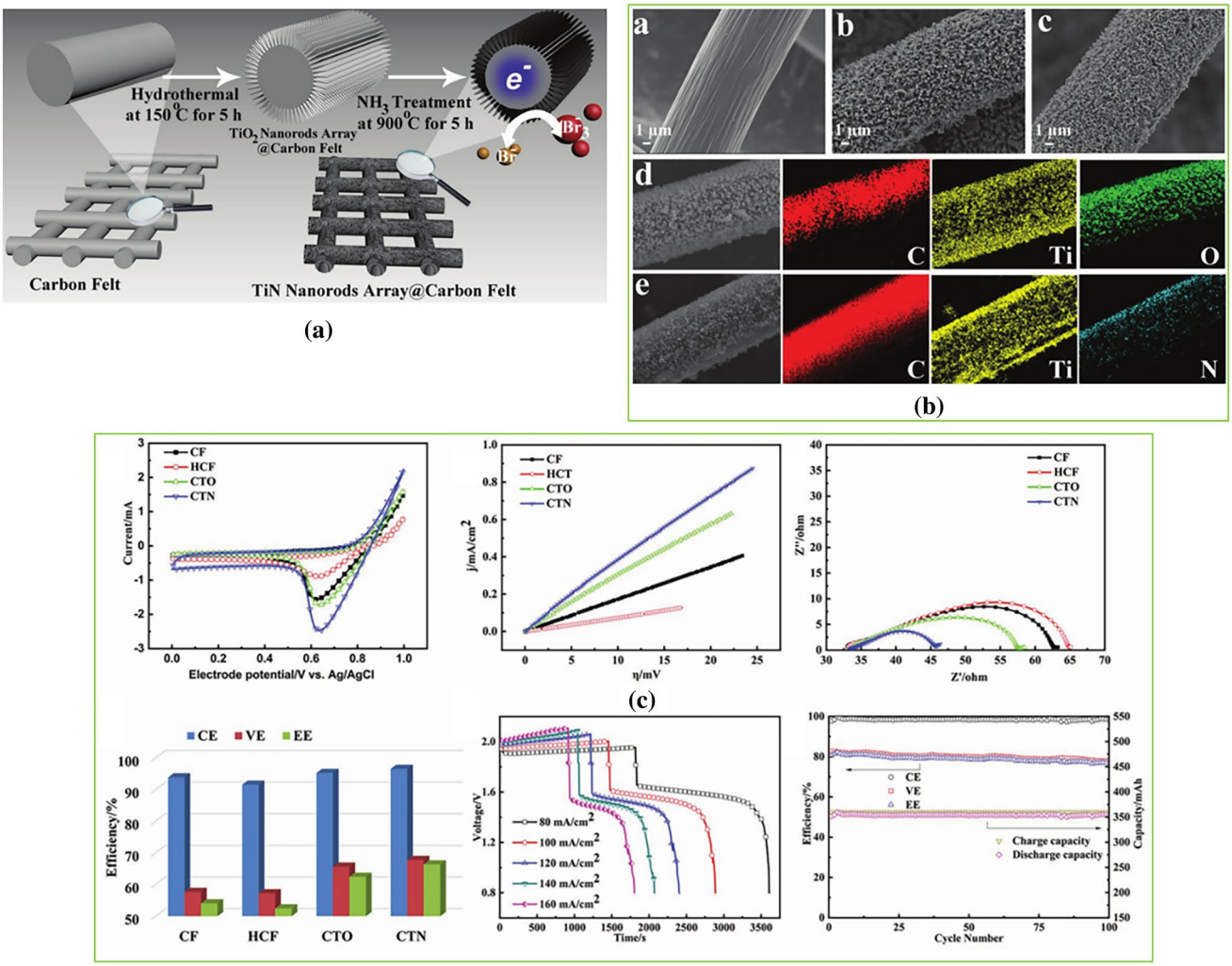

Figure 12. (a) Schematic illustration of the fabrication of a carbon felt-supported TiN nanorod array 3D hierarchical composite electrode. (b) SEM images and EDS mappings of the CF, CTO, and CTN. (c) The electrochemical performance of CF, HCF, CTO, and CTN together with ZBFB with CTN.[108] Adapted from Ref [108].

as high as 94%, an ultra-long cycling life over 11,000 cycles, and the suppressed self-discharge rate.

Zn–Ni(OH)$_2$ battery

Among various aqueous rechargeable batteries, alkaline aqueous Zn–Ni(OH)$_2$ battery (Ni–Zn battery) shows great potential for the advantages of high safety and resource abundance.[12,13,16,85,86] The redox reaction taking place in cathode can be formulated as follows: $NiOOH + e^- + H_2O \leftrightarrow Ni(OH)_2 + OH^-$.[110,111] However, the large-scale application of Ni–Zn batteries are restricted by the poor durability, which is mainly originated from the Zn dendrite on anode and the irreversibility of Ni-based cathode.[112] Particularly, high-energy Ni–Zn batteries have been beset by the limited capacity density, slow mass transfer, poor electronic conductivity, and utilization efficiency of the Ni cathode. To address these issues, numerous attempts have been imposed on the design of Ni-based cathodes. The nickel–cobalt double hydroxides (NiCo-DH) as a high-rate cathode for Ni–Zn battery have been prepared by Chen et al.[113] Compared with single metal oxides, double hydroxides can provide more active sites. The cathode exhibits a three-dimensional architecture composed of hierarchical micro-nano sheets, which provides more active sites and facilitates ion diffusion (Fig. 14a). Besides Ni-based cathode mechanism, the NiCo-DH electrodes also deliver a redox reaction that can be formulated as follows: $Co(OH)_2 + OH^- \leftrightarrow CoOOH + H_2O + e^-$. Due to these properties, a high specific capacity of 329 mAh g^{-1} and high Coulombic efficiencies of 99.5% are displayed, as illustrated in Fig. 14b and c. Although the favorable electrochemical performance can be obtained, the Co-based electrodes will cause the cost increasing. Thus, in order to obtain Co-free cathode, Chao et al. have developed a facile top-down strategy to synthesize Co-free Ni-based microspheres, which are coated by NiS as cathodes for Ni–Zn batteries (Fig. 15a).[114] Based on the anion exchange reaction and the Kirkendall effect, the Ni cathode endows stable and uniform NiS nanodots, which constructs a radial network of microstructures

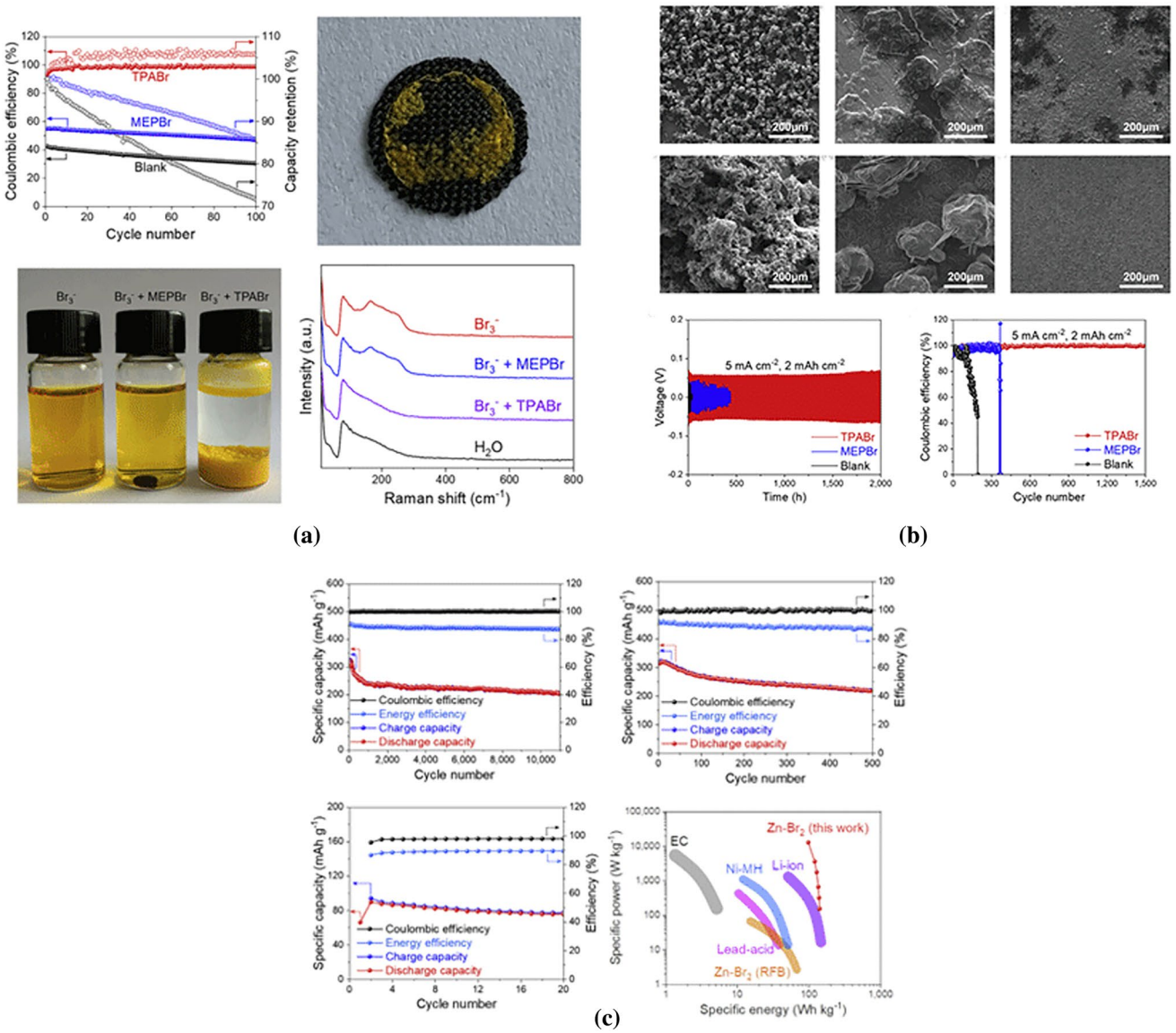

Figure 13. (a) The properties of bromine complexing agents with blank, MEPBr, and TPABr electrolytes. (b) The zinc plating/stripping behaviors in blank, MEPBr, and TPABr electrolytes. (c) Electrochemical performances of the zinc–bromine static batteries with the CMK-3 electrode.[109] Adapted from Ref [109].

with abundant interconnected mesopores in Fig. 15b. As a proof of concept, the Ni-Zn pouch battery with a commercial-grade 3.5 Ah is developed, which shows gravimetric energy densities of 165 Wh kg^{-1} and volumetric energy densities of 506 Wh L^{-1} (Fig. 15c). In addition, a low discharge pulse voltage (1.74 V) and high charge pulse voltage (1.84 V) are delivered in Fig. 15d, which show a small pulse polarization. Moreover, NiS shows high electric conduction, which can obtain Co-free cathode. The cost comes down, and more favorable electrochemical performance is achieved, which exhibits ultra-long high current pulses of 80,000 cycles (Fig. 15e). Thus, a high areal capacity of 41.3 mAh cm^{-2} and an impressive power response of 715 mW cm^{-2} are displayed in the proposed Ni-Zn battery. From the above-mentioned discussions, the special structure, such as 3D architecture and porous structure, can display fast ion diffusion and provide numerous active sites to achieve stable cathodes with high capacity. A simple, efficient, and scalable method have been developed to prepare 3D Ni@NiO core–shell electrode based on commercial nickel foam by Lu et al. (Fig. 16a).[115] The NiO layer in situ growing on Ni foam exhibits highly reversible redox reaction and presents interaction with Ni, which delivers beneficial cycling stability. Moreover, the fast ion diffusion and high conductivity are facilitated by the 3D skeleton, which facilitate to achieve the encouraged electrochemical performance (Fig. 16b). Moreover, the 92.5% retention of initial capacity and Coulombic efficiency of 100% are shown at 8 mA cm^{-2} after 1800 cycles (Fig. 16c). The slow mass transfer and poor electronic conductivity dominate the main issues of Ni-based cathode, which would result in the low practical capacity in Ni-Zn battery. To tackle the issues, electrodes endowing special structure, such as 3D

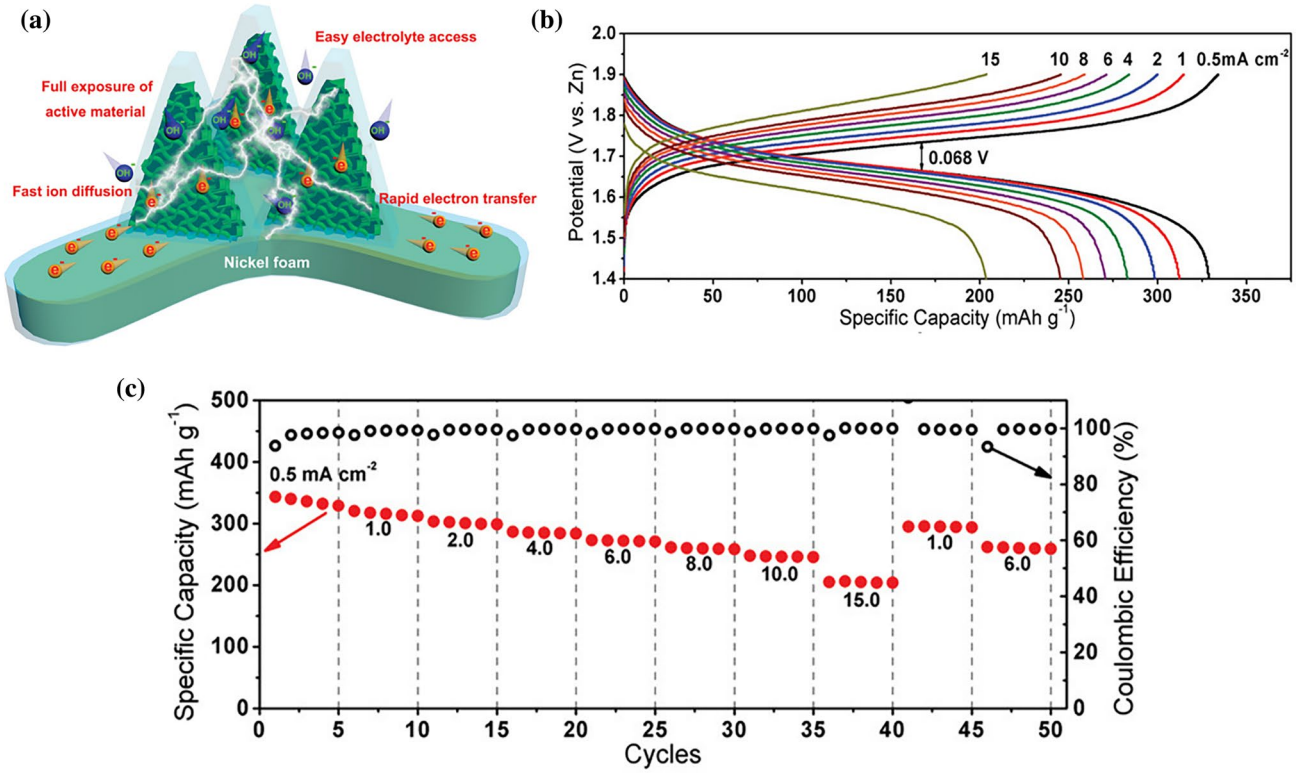

Figure 14. (a) Schematic diagram of the electrochemical performance output NiCo-DH electrode. (b) Charge/discharge curves at the different current densities. (c) Specific capacities of the as-assembled Ni–Zn battery.[113] Adapted from Ref [113].

structure and nanofiber network, are employed, which can not only enhance ion and electron transports but also improve the active mass loading for Ni–Zn battery.[116,117]

Ni(OH)$_2$ cathode-based batteries

As one of the commercial energy storage and conversion technology, the nickel metal hydride (Ni–MH) batteries show high specific energy, long cycle life, favorable environment, and so on, which have been widely used in all kinds of portable electronic products and electric vehicle (EV).[118–120] The typical electrochemical reactions taking placing in a Ni–MH battery can be presented according to the following equations (Eqs. 10 to 12):

$$\text{Cathode: } Ni(OH)_2 + OH^- \leftrightarrow NiOOH + H_2O + e^- \quad (10)$$

$$\text{Anode: } M + H_2O + e^- \leftrightarrow MH + OH^- \quad (11)$$

$$\text{Overall: } Ni(OH)_2 + M \leftrightarrow NiOOH + MH. \quad (12)$$

Upon charging, the metal hydride and hydroxyl ions can be obtained at the anode through the reactions between the hydrogen storage alloy and water. Meanwhile, Ni(OH)$_2$ would be oxidized to NiOOH at the cathode. The above reactions would take place reversibly on discharging. From the overall reaction presented above, it can be found that the hydrogen transfers from cathode to anode and returns reversibly during charge/discharge process without the participation of electrolyte, respectively.

Although larger achievements have been obtained, numerous challenges are required to be addressed for the further developments. The electrochemical performance of Ni–MH batteries strongly depends on the inherent characteristics of electrode active materials; meanwhile, the electrochemical reaction kinetics of hydrogen storage alloy are significant. Generally, the pressure–composition isotherms (*P*–*C*–*T*) can be used to determine the hydrogen capacity, moderate hydride stability, and metal-to-hydrogen (M–H) bond strength.[121] Currently, the hydrogen storage alloy mainly contains expensive cobalt mental, resulting in high cost. Therefore, the development of hydrogen storage alloys for Ni–MH batteries is urgent. The rare earth-based AB_5-type alloys deliver low self-discharge performance. However, it shows low capacity and poor cycling lifetimes. The strategies including A-site substitution, B-site substitution, non-stoichiometric additives, alloy nanocrystallization, and surface treatment are employed to improve the electrochemical performance of AB_5-type alloy.[122,123] The Ti- and Zr-based AB_2-type alloys show higher energy density and longer cycling life compared to AB_5-type alloys. Whereas AB_2-type alloys are limited by the slow activation together with low-rate capabilities. The introduction of the secondary phase with favorable electrochemical catalytic activity would further enhance the electrochemical properties of the AB_2-type alloys.[124,125] Meanwhile, the Mg-based alloys present the advantages of low cost and abundant nature resources. Nevertheless, the practical applications of Mg-based alloys

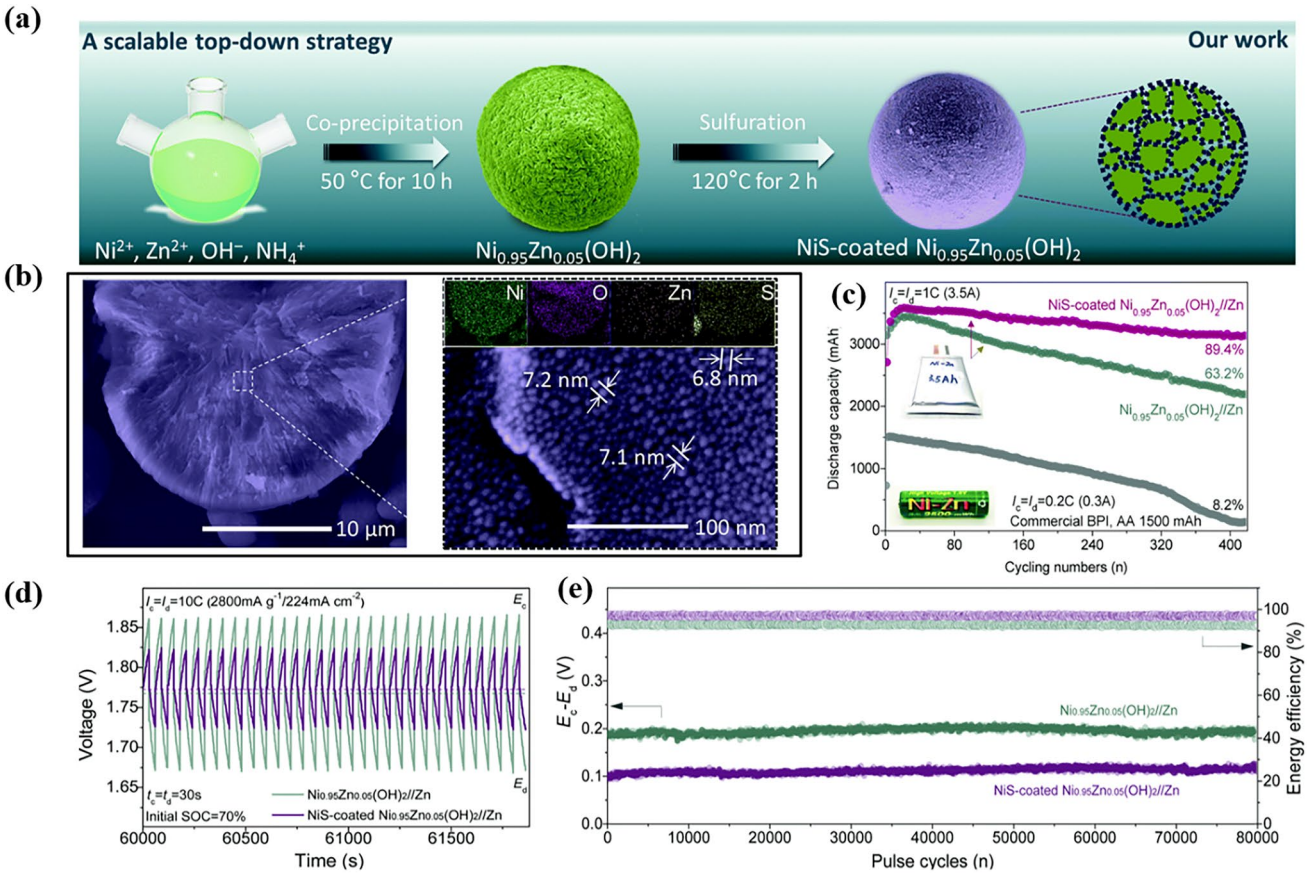

Figure 15. (a) Schematic diagram of the top-down strategy. (b) Cross-section SEM images of the inner structure of electrode. (c) Cycling performance of the 3.5-Ah pouch-type Ni–Zn battery. Electrochemical performance of the Ni–Zn battery during the pulse charge/discharge cycles: (d) voltage profiles at 10 C and (e) voltage difference and energy efficiency.[114] Adapted from Ref [114].

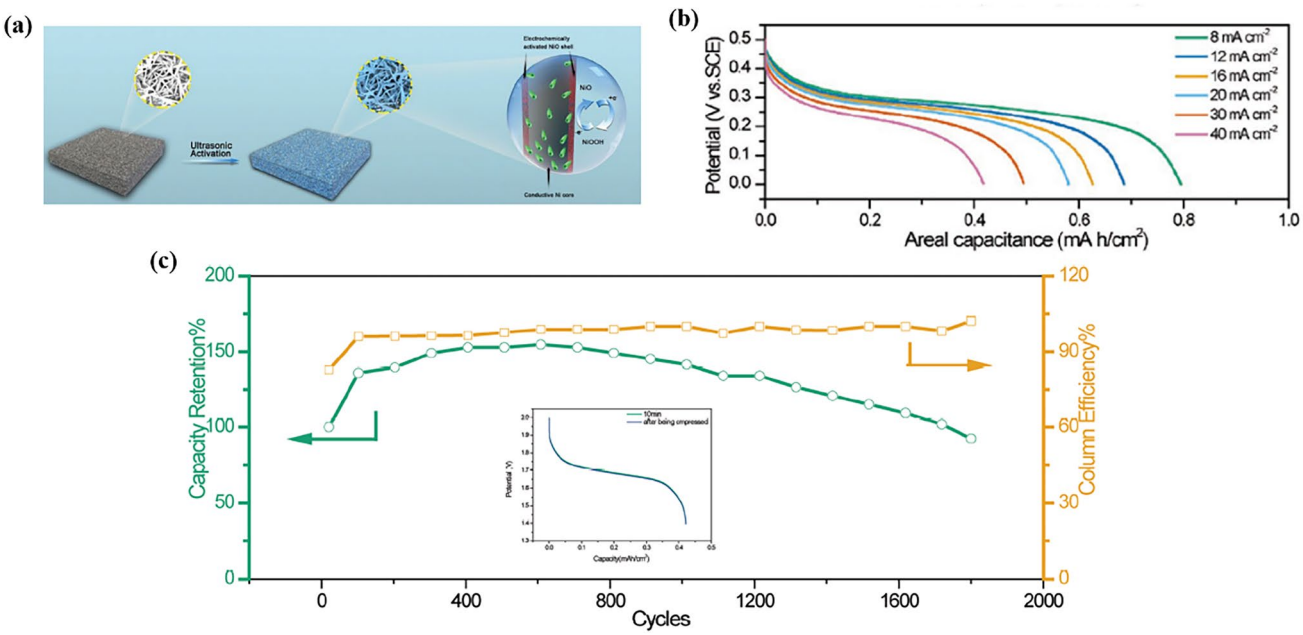

Figure 16. (a) Schematic diagram of the electrode formation. (b) Galvanostatic discharge curves of the electrode at various current densities. (c) Cycling performance of the Ni–Zn battery at 8 mA cm^{-2} for 1800 cycles.[115] Adapted from Ref [115].

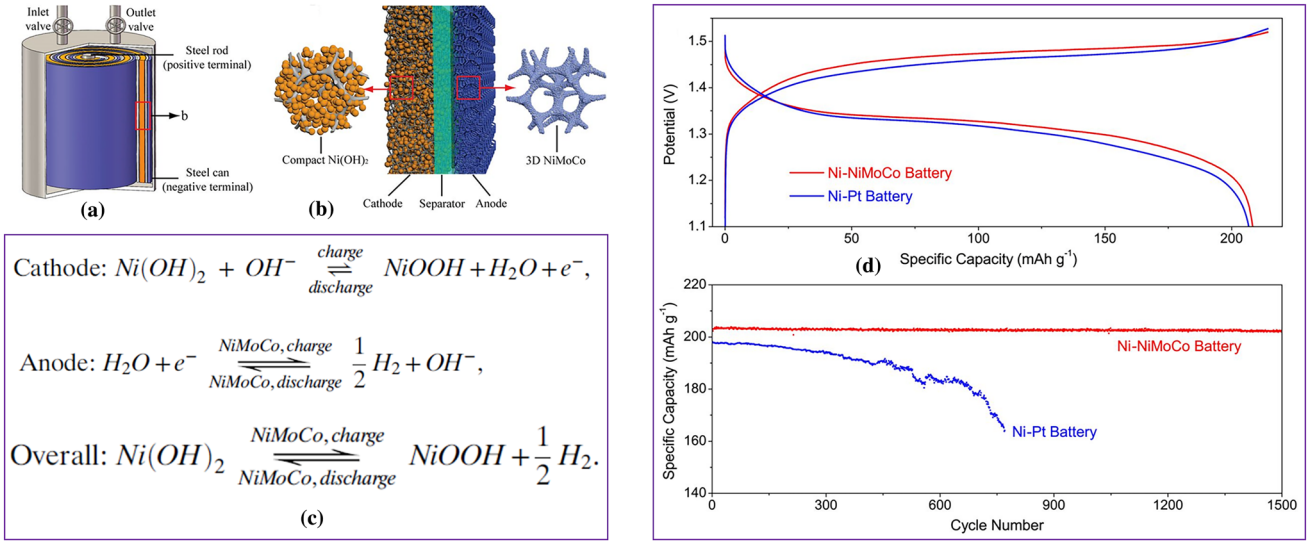

Figure 17. The Ni–H cylindrical battery: (a) schematic design, (b) electrode configuration, (c) redox reactions, and (d) the electrochemical performance.[136] Adapted from Ref [136].

are limited by their unfavorable hydrogenation/dehydrogenation kinetics and rapid degradation at room temperature. The nanocrystallization and amorphization have been considered to be appealing strategies for activating the Mg-based alloy.[126–128] In addition, the superlattice alloys show high energy/power density, but the high stability of their hydride results in the slow hydrogenolysis at room temperature. Simultaneously, the alloy pulverization and the oxidation of Mg and La would take place in alkaline solution. The strategies through the preparation of multicomponent compounds, composition optimization, ball-milling treatment, surface treatment, and heat treatment are widely used to improve the electrochemical performance of superlattice alloys.[129,130] Due to their high discharge capacities, the Ti–V-based multicomponent multiphase alloys have been developed as the promising candidate for Ni–MH batteries owing to their high discharge capacities. Because of the alloy pulverization and corrosion of alloy compositions, the cycling life of these alloys are still unfavorable. The composition optimization, employment of additives, and surface treatment are widely used to address the above issues.[131–133]

As a cathode active material, $Ni(OH)_2$ has been widely employed in Ni–MH, Ni–Cd batteries, and asymmetric supercapacitor. At present, the Ni–MH batteries are operated based on the conversion between β-$Ni(OH)_2$ and β-NiOOH. The actual electrochemical capacity of β-$Ni(OH)_2$ is close to theory value (289 mAh g^{-1}). Compared to β-$Ni(OH)_2$, the α-$Ni(OH)_2$ shows larger capacity (482 mAh g^{-1}). α-$Ni(OH)_2$ displays higher discharge voltage and flatter discharge platform, attracting extensive attention. However, due to the problems including poor stability in strongly alkaline solutions, low packing density, and the conversion to β-$Ni(OH)_2$, the application of α-$Ni(OH)_2$ is restricted. The substitution reactions that partial nickel ion are replaced by high valent mental ions (Al^{3+}, Fe^{3+}, Mn^{3+}, etc.) and the doping of interlayer anions would improve the electrochemical performance of α-$Ni(OH)_2$.[134,135] Cui's group has introduced a concept of nickel–hydrogen battery on basis of $Ni(OH)_2$/NiOOH redox cathode and H^+/H_2 gas anode, respectively, which can be achieved through the construction based on a custom-made cylindrical cell.[136] The NiMoCo-catalyzed anode, polymer separator, and rolling $Ni(OH)_2$ cathode are used to assemble into a steel vessel. The micrometer-sized $Ni(OH)_2$ spheres coated on nickel foam have been used as cathode with the aim to develop a compact electrode. The $Ni(OH)_2$ cathode would be oxidized to NiOOH. Meanwhile, the hydrogen gas is produced on the anode due to the NiMoCo-catalyzed HER in alkaline electrolyte during charge process. The above reactions can be taken placed reversibly during discharge process, in which the $Ni(OH)_2$ and H^+ are obtained. The comparable electrochemical behaviors have been presented via the employment of the NiMoCo and Pt/C anodes of Swagelok Ni–H battery. Moreover, the favorable long-term cycle life (over 1500 cycles) with negligible capacity decay can be obtained by the Swagelok Ni–NiMoCo battery, while the Ni–Pt battery displays obvious capacity degradation over cycling, which could be attributed to the partial Pt/C catalysts detached from the anode during cycling. The energy density of ~140 Wh kg^{-1} can be achieved by this proposed nickel–hydrogen battery, which demonstrates the appealing application for large-scale energy storage (Fig. 17).

Instead of employing metal hydride (MH) as anode for Ni–MH batteries, Yao et al.[137] have developed quinones as stable anode coupled with $Ni(OH)_2$ for Ni–MH batteries. The quinones can store charge through an 'ion-coordination' mechanism, in which the electronegative oxygen atoms can be coordinated with the cations upon reduction process and uncoordinated reversibly during the reverse oxidation process. When the anthraquinone-based polymer, poly(anthraquinonyl sulfide) (PAQS), is used as

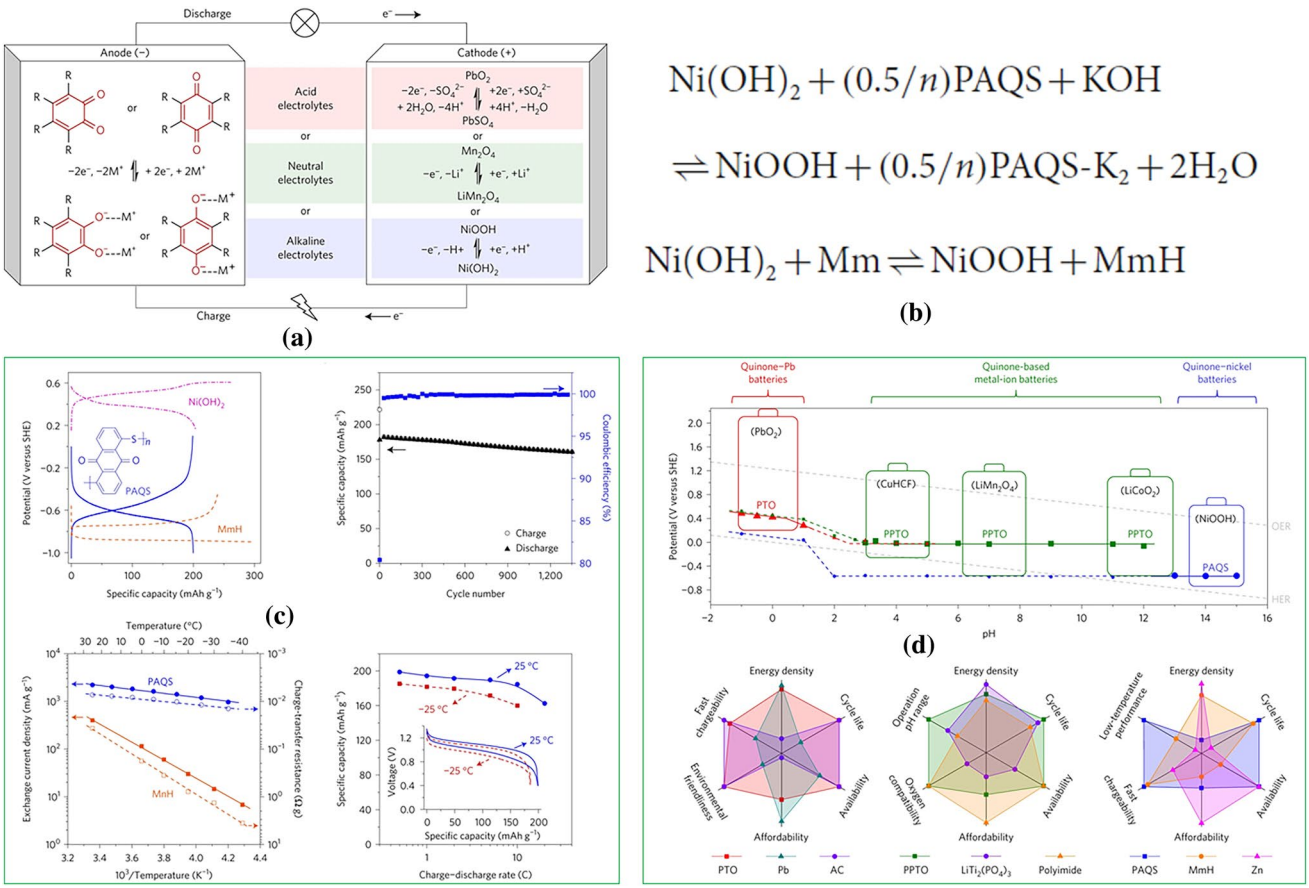

Figure 18. (a) Schematics of the aqueous rechargeable batteries on basis of quinone anodes and corresponding redox chemistries. (b) The reactions presented for $Ni(OH)_2$-PAQS and $Ni(OH)_2$–MH. (c) The electrochemical performance of quinone-based alkaline batteries. (d) The comparison of various anode materials for advanced aqueous batteries.[137] Adapted from Ref [137].

anode material for Ni–MH battery, it delivers a specific capacity of 200 mAh g^{-1} in KOH electrolyte. Despite the inferior specific energy density of $Ni(OH)_2$-PAQS to that of Ni–MH ascribed to the consumption of the KOH electrolyte, there is much room for further enhancement in the specific energy density of $Ni(OH)_2$-PAQS obtained by developing novel quinone anodes with lower reduction potential. Generally, the PAQS displays negligible performance dependence on temperature due to lower activation energy, and the proposed $Ni(OH)_2$-PAQS battery shows a high capacity retention. These remarkable properties enable PAQS to achieve favorable electrochemical performance at low temperatures. From the Pourbaix diagram presenting the reduction potential versus pH of PAQS electrodes, it is found that the PAQS potential approaches the HER potential at each pH value and there is room for further improvement. Compared with other commercial and emerging anode materials, the PAQS displays a long cycling life and environmental friendliness for the absence of heavy metals; meanwhile, their intrinsic merits, such as efficient charge transport and fast electrode kinetics, ensure fast chargeability and high power density even at low temperatures, which can address some of the major challenges for Ni–MH batteries (Fig. 18).

Conclusion

With the increasing demand for large-scale ESSs applications, ARBs have attracted intensive attention owing to numerous advantages of aqueous electrolytes, including lower cost, superior security, and higher power density. Although great achievements have been obtained in ARBs, a series of challenges are required to address as follows. (i) H_2 and O_2 evolution: The electrochemical window of aqueous electrolytes is quite narrow (~ 1.23 V). Beyond this, the H_2 and O_2 evolution would take place. (ii) Side reactions: The structural stability of active materials could be degraded in the electrolyte solutions with the presence of dissolved O_2. Furthermore, some undesired reaction would occur between the intercalated metal ions in the host materials and H_2O or dissolved O_2. (iii) Electrode dissolution: During the electrochemical operations at various pH, the dissolution of electrode in aqueous electrolyte would occur. To address the issues of electrode dissolution, the surface coating and the employment of surface stabilizers are the effective methods. (iv) Proton co-insertion: During the intercalation of metal ions into the host materials, the co-insertion of proton can be observed, which would change the pH of aqueous

electrolytes. Therefore, substantial research efforts are required to develop electrode materials with negligible proton co-insertion. (v) Metal reversibility: As the promising metal anode, the poor reversibility is still a bottleneck for the development of zinc anode-based systems, which is mainly caused from the issues, including dendrite growth, corrosion, passivation, and shape change. (vi) High cost and limited capacity: When the new $Ni(OH)_2$ cathode-based batteries are widely developed, the cost of electrocatalysts used for H^+/H_2 anode and the limited capacities of organic composite anodes are suggested to consider. In order to facilitate the further development of ARBs, several strategies are proposed. First, the developments of electrochemical active material for ARBs together with the investigations on the underlying reactive mechanism are significant. Second, the ARBs systems including anode, electrolyte, and cathode are suggested to optimize and achieve the desired electrochemical performance. Third, the fabrication techniques of ARBs cannot be neglected, such as O_2 elimination, which would promote the application of ARBs. Although the numerous challenges are still remained, the future large-scale energy storage applications based on ARBs are deserved to expect.

Acknowledgments

We are grateful for the partial financial support from the National Natural Science Foundation of China (Grant Nos. 21935003 and 22075171).

Data availability

All data generated or analyzed during this study are included in this published article and its supplementary information files.

Declarations

Conflict of interest

The authors declare no conflict of interest.

REFERENCES

1. J.Y. Luo, W.J. Cui, P. He, Y.Y. Xia, Nat. Chem. **2**, 760 (2010)
2. Y. Wang, Y. Xia, Nat. Chem. **5**, 445 (2013)
3. Y. Qiao, J. Yi, S. Wu, Y. Liu, S. Yang, P. He, H. Zhou, Joule **1**, 359 (2017)
4. K. Wu, F. Ning, J. Yi, X. Liu, J. Qin, Y. Liu, J. Zhang, J. Energy Chem. **69**, 237 (2022)
5. Q. Li, L. Han, Q. Luo, X. Liu, J. Yi, Batter. Supercaps **5**, e202100417 (2022)
6. J. Yi, Y. Liu, Y. Qiao, P. He, H. Zhou, ACS Energy Lett. **2**, 1378 (2017)
7. X. Liu, J. Yi, K. Wu, Y. Jiang, Y. Liu, B. Zhao, W. Li, J. Zhang, Nanotechnology **31**, 122001 (2020)
8. J. Huang, Y. Xie, L. Yan, B. Wang, T. Kong, X. Dong, Y. Wang, Y. Xia, Energy Environ. Sci. **14**, 883 (2021)
9. R. Hu, Y. Fang, X. Liu, K. Zhu, D. Cao, J. Yi, G. Wang, Chem. Res. Chin. Univ. **37**, 311 (2021)
10. J. Yi, S. Wu, S. Bai, Y. Liu, N. Li, H. Zhou, J. Mater. Chem. A **4**, 2403 (2016)
11. S. Wu, J. Yi, K. Zhu, S. Bai, Y. Liu, Y. Qiao, M. Ishida, H. Zhou, Adv. Energy Mater. **7**, 1601759 (2017)
12. J. Cui, X. Liu, Y. Xie, K. Wu, Y. Wang, Y. Liu, J. Zhang, J. Yi, Y. Xia, Mater. Today. Energy **18**, 100563 (2020)
13. X. Liu, Y. Fang, P. Liang, J. Xu, B. Xing, K. Zhu, Y. Liu, J. Zhang, J. Yi, Chin. Chem. Lett. **32**, 2899 (2021)
14. J. Huang, Z. Guo, Y. Ma, D. Bin, Y. Wang, Y. Xia, Small Methods **3**, 1800272 (2019)
15. P. Liang, J. Yi, X. Liu, K. Wu, Z. Wang, J. Cui, Y. Liu, Y. Wang, Y. Xia, J. Zhang, Adv. Funct. Mater. **30**, 1908528 (2020)
16. C. Xu, Y. Zhang, N. Zhang, X. Liu, J. Yi, X. Liu, X. Lu, Q. Ru, H. Lu, X. Peng, X.S. Zhao, J. Ma, Chem. - Asian J. **15**, 3696 (2020)
17. Y. Wang, J. Yi, Y. Xia, Adv. Energy Mater. **2**, 830 (2012)
18. J. Huang, L. Yan, D. Bin, X. Dong, Y. Wang, Y. Xia, J. Mater. Chem. A **8**, 5959 (2020)
19. F. Wang, O. Borodin, T. Gao, X. Fan, W. Sun, F. Han, A. Faraone, J.A. Dura, K. Xu, C. Wang, Nat. Mater. **17**, 543 (2018)
20. L. Chen, J.L. Bao, X. Dong, D.G. Truhlar, Y. Wang, C. Wang, Y. Xia, ACS Energy Lett. **2**, 1115 (2017)
21. W. Li, J.R. Dahn, D.S. Wainwright, Science **264**, 1115 (1994)
22. Y. Wen, Y. Liu, D. Bin, Z. Wang, C. Wang, Y. Cao, X. Ai, Y. Xia, Sci. China: Chem. **62**, 118 (2019)
23. Z. Guo, L. Chen, Y. Wang, C. Wang, Y. Xia, ACS Sustain. Chem. Eng. **5**, 1503 (2017)
24. X. Dong, L. Chen, X. Su, Y. Wang, Y. Xia, Angew. Chem. Int. Ed. **55**, 7474 (2016)
25. J.Y. Luo, Y.Y. Xia, Adv. Funct. Mater. **17**, 3877 (2007)
26. Y. Wang, L. Chen, Y. Wang, Y. Xia, Electrochim. Acta **173**, 178 (2015)
27. F. Wang, L. Suo, Y. Liang, C. Yang, F. Han, T. Gao, W. Sun, C. Wang, Adv. Energy Mater. **7**, 1600922 (2016)
28. P. He, J.L. Liu, W.J. Cui, J.Y. Luo, Y.Y. Xia, Electrochim. Acta **56**, 2351 (2011)
29. F. Wang, Y. Lin, L. Suo, X. Fan, T. Gao, C. Yang, F. Han, Y. Qi, K. Xu, C. Wang, Energy Environ. Sci. **9**, 3666 (2016)
30. X. Gu, J.L. Liu, J.H. Yang, H.J. Xiang, X.G. Gong, Y.Y. Xia, J. Phys. Chem. C **115**, 12672 (2011)
31. Y. Wang, J. Lou, W. Wu, C. Wang, Y. Xia, J. Electrochem. Soc. **154**, A228 (2007)
32. C. Han, W. Li, H.-K. Liu, S. Dou, J. Wang, Mater. Horiz. **6**, 1812 (2019)
33. D.A. Kuznetsov, B. Han, Y. Yu, R.R. Rao, J. Hwang, Y. Román-Leshkov, Y. Shao-Horn, Joule **2**, 225 (2018)
34. I.B. Stojković, N.D. Cvjetićanin, S.V. Mentus, Electrochem. Commun. **12**, 371 (2010)
35. L. Suo, O. Borodin, T. Gao, M. Olguin, J. Ho, X. Fan, C. Luo, C. Wang, K. Xu, Science **350**, 938 (2015)
36. Y.G. Wang, Y.Y. Xia, Electrochem. Commun. **7**, 1138 (2005)
37. Y.G. Wang, J.Y. Luo, C.X. Wang, Y.Y. Xia, J. Electrochem. Soc. **153**, A1425 (2006)
38. Yg. Wang, Yy. Xia, J. Electrochem. Soc. **153**, A450 (2006)
39. Z. Guo, Y. Zhao, Y. Ding, X. Dong, L. Chen, J. Cao, C. Wang, Y. Xia, H. Peng, Y. Wang, Chem **3**, 348 (2017)
40. L. Chen, J. Liu, Z. Guo, Y. Wang, C. Wang, Y. Xia, J. Electrochem. Soc. **163**, A904 (2016)
41. S. Guo, J. Yi, Y. Sun, H. Zhou, Energy Environ. Sci. **9**, 2978 (2016)
42. D. Bin, F. Wang, A.G. Tamirat, L. Suo, Y. Wang, C. Wang, Y. Xia, Adv. Energy Mater. **8**, 1703008 (2018)
43. S. Guo, P. Liu, Y. Sun, K. Zhu, J. Yi, M. Chen, M. Ishida, H. Zhou, Angew. Chem. Int. Ed. **54**, 11–701 (2015)
44. K. Zhu, S. Guo, J. Yi, S. Bai, Y. Wei, G. Chen, H. Zhou, J. Mater. Chem. A **3**, 22012 (2015)
45. S. Guo, Y. Sun, J. Yi, K. Zhu, P. Liu, Y. Zhu, G. Zhu, M. Chen, M. Ishida, H. Zhou, NPG Asia Mater. **8**, e266 (2016)
46. W. Wang, X. Liu, Q. Xu, H. Liu, Y. Wang, Y. Xia, Y. Cao, X. Ai, J. Mater. Chem. A **6**, 4354 (2018)
47. J. Liu, Y. Liu, Y. Wang, C. Wang, Y. Xia, Batter. Supercaps **2**, 867 (2019)
48. Y. Lv, Q. He, X. He, Y. Wang, J. Yi, H. Ji, Chem. Commun. **56**, 5182 (2020)
49. Y. Liu, J. Liu, Y. Wu, D. Bin, S. Bo, Y. Wang, Y. Xia, ACS Appl. Energy Mater. **1**, 5151 (2018)

50. H. Xia, Y.S. Meng, G. Yuan, C. Cui, L. Luc, Electrochem. Solid-State Lett. **15**, A60 (2012)
51. M. Toupin, T. Brousse, D. Belanger, Chem. Mater. **16**, 3184 (2004)
52. J.F. Whitacre, A. Tevar, S. Sharma, Electrochem. Commun. **12**, 463 (2010)
53. Y. Wang, L. Mu, J. Liu, Z. Yang, X. Yu, L. Gu, Y.-S. Hu, H. Li, X.-Q. Yang, L. Chen, X. Huang, Adv. Energy Mater. **5**, 1501005 (2015)
54. Y.H. Jung, S.-T. Hong, D.K. Kim, J. Electrochem. Soc. **160**, A897 (2013)
55. X. Liu, L. Tang, Z. Li, J. Zhang, Q. Xu, H. Liu, Y. Wang, Y. Xia, Y. Cao, X. Ai, J. Mater. Chem. A **7**, 18940 (2019)
56. L. Tang, X. Liu, Z. Li, X. Pu, J. Zhang, Q. Xu, H. Liu, Y. Wang, Y. Xia, ACS Appl. Mater. Interfaces **11**, 27813 (2019)
57. Y. Cao, C. Yang, Y. Liu, X. Xia, D. Zhao, Y. Cao, H. Yang, J. Zhang, J. Lu, Y. Xia, ACS Energy Lett. **5**, 3788 (2020)
58. L. Tang, J. Zhang, Z. Li, X. Liu, Q. Xu, H. Liu, Y. Wang, Y. Xia, Z. Ma, J. Power Sources **451**, 227734 (2020)
59. Y. Cao, Y. Liu, D. Zhao, J. Zhang, X. Xia, T. Chen, L.-C. Zhang, P. Qin, Y. Xia, J. Alloys Compd. **784**, 939 (2019)
60. F. Sanz, C. Parada, J.M. Rojo, C. Ruiz-Valero, Chem. Mater. **13**, 1334 (2001)
61. M. Nose, H. Nakayama, K. Nobuhara, H. Yamaguchi, S. Nakanishi, H. Iba, J. Power Sources **234**, 175 (2013)
62. J.Y. Jang, H. Kim, Y. Lee, K.T. Lee, K. Kang, N.S. Choi, Electrochem. Commun. **44**, 74 (2014)
63. M. Nose, S. Shiotani, H. Nakayama, K. Nobuhara, S. Nakanishi, H. Iba, Electrochem. Commun. **34**, 266 (2013)
64. W. Song, X. Ji, Y. Zhu, H. Zhu, F. Li, J. Chen, F. Lu, Y. Yao, C.E. Banks, ChemElectroChem **1**, 871 (2014)
65. J.-H. Lee, G. Ali, D.H. Kim, K.Y. Chung, Adv. Energy Mater. **7**, 1601491 (2017)
66. L. Chen, W. Sun, K. Xu, Q. Dong, L. Zheng, J. Wang, D. Lu, Y. Shen, J. Zhang, F. Fu, H. Kong, J. Qin, H. Chen, ACS Energy Lett. **7**, 1672 (2022)
67. J. Han, A. Mariani, H. Zhang, M. Zarrabeitia, X. Gao, D.V. Carvalho, A. Varzi, S. Passerini, Energy Storage Mater. **30**, 196 (2020)
68. M. Minakshi, D. Meyrick, D. Appadoo, Energy Fuels **27**, 3516 (2013)
69. X. Dong, L. Chen, J. Liu, S. Haller, Y. Wang, Y. Xia, Sci. Adv. **2**, e1501038 (2016)
70. Z. Li, W. Shen, C. Wang, Q. Xu, H. Liu, Y. Wang, Y. Xia, J. Mater. Chem. A **8**, 24212 (2020)
71. T. Song, H. Chen, Q. Xu, H. Liu, Y. Wang, Y. Xia, ACS Appl. Mater. Interfaces **10**, 37163 (2018)
72. Y. Cao, Y. Liu, T. Chen, X. Xia, L. Zhang, J. Zhang, Y. Xia, Ionics **25**, 1083 (2019)
73. S.I. Park, I. Gocheva, S. Okada, J. Yamaki, J. Electrochem. Soc. **158**, A1067 (2011)
74. Q. Zhao, Y. Lu, J. Chen, Adv. Energy Mater. **7**, 1601792 (2017)
75. Y. Yamada, K. Usui, K. Sodeyama, S. Ko, Y. Tateyama, A. Yamada, Nat. Energy **1**, 16129 (2016)
76. H. Qin, Z.P. Song, H. Zhan, Y.H. Zhou, J. Power Sources **249**, 367 (2014)
77. R.-S. Kuehnel, D. Reber, C. Battaglia, ACS Energy Lett. **2**, 2005 (2017)
78. Z. Guo, Y. Ma, X. Dong, J. Huang, Y. Wang, Y. Xia, Angew. Chem. Int. Ed. **57**, 11737 (2018)
79. Z. Wang, J. Huang, Z. Guo, X. Dong, Y. Liu, Y. Wang, Y. Xia, Joule **3**, 1289 (2019)
80. D. Bin, Y. Liu, B. Yang, J. Huang, X. Dong, X. Zhang, Y. Wang, Y. Xia, ACS Appl. Mater. Interfaces **11**, 20796 (2019)
81. X. Pu, T. Song, L. Tang, Y. Tao, T. Cao, Q. Xu, H. Liu, Y. Wang, Y. Xia, J. Power Sources **437**, 226917 (2019)
82. Y. Tao, Z. Li, L. Tang, X. Pu, T. Cao, D. Cheng, Q. Xu, H. Liu, Y. Wang, Y. Xia, Electrochim. Acta **331**, 135296 (2020)
83. N. Wang, Y. Yang, X. Qiu, X. Dong, Y. Wang, Y. Xia, Chemsuschem **13**, 5556 (2020)
84. D. Bin, Y. Wang, A.G. Tamirat, P. Zhu, B. Yang, J. Wang, J. Huang, Y. Xia, ACS Sustainable Chem. Eng. **9**, 3223 (2021)
85. J. Cui, Z. Guo, J. Yi, X. Liu, K. Wu, P. Liang, Q. Li, Y. Liu, Y. Wang, Y. Xia, J. Zhang, Chemsuschem **13**, 2160 (2020)
86. K. Wu, J. Yi, X. Liu, Y. Sun, J. Cui, Y. Xie, Y. Liu, Y. Xia, J. Zhang, Nano-Micro Lett. **13**, 79 (2021)
87. J. Yang, B. Yin, Y. Sun, H. Pan, W. Sun, B. Jia, S. Zhang, T. Ma, Nano-Micro Lett. **14**, 42 (2022)
88. J. Yi, P. Liang, X. Liu, K. Wu, Y. Liu, Y. Wang, Y. Xia, J. Zhang, Energy Environ. Sci. **11**, 3075 (2018)
89. J. Hao, X. Li, X. Zeng, D. Li, J. Mao, Z. Guo, Energy Environ. Sci. **13**, 3917 (2020)
90. F. Mo, N. He, L. Chen, M. Li, S. Yu, J. Zhang, W. Wang, J. Wei, Front. Chem. **9**, 822624 (2021)
91. J. Huang, Z. Wang, M. Hou, X. Dong, Y. Liu, Y. Wang, Y. Xia, Nat. Commun. **9**, 2906 (2018)
92. K. Wu, J. Huang, J. Yi, X. Liu, Y. Liu, Y. Wang, J. Zhang, Y. Xia, Adv. Energy Mater. **10**, 1903977 (2020)
93. D. Bin, W. Huo, Y. Yuan, J. Huang, Y. Liu, Y. Zhang, F. Dong, Y. Wang, Y. Xia, Chem **6**, 968 (2020)
94. J. Yi, X. Liu, P. Liang, K. Wu, J. Xu, Y. Liu, J. Zhang, Organometallics **38**, 1186 (2019)
95. D. Bin, Z. Guo, A.G. Tamirat, Y. Ma, Y. Wang, Y. Xia, Nanoscale **9**, 11148 (2017)
96. Z. Guo, C. Li, W. Li, H. Guo, X. Su, P. He, Y. Wang, Y. Xia, J. Mater. Chem. A **4**, 6282 (2016)
97. D. Bin, B. Yang, C. Li, Y. Liu, X. Zhang, Y. Wang, Y. Xia, ACS Appl. Mater. Interfaces **10**, 26178 (2018)
98. Z. Guo, F. Wang, Y. Xia, J. Li, A.G. Tamirat, Y. Liu, L. Wang, Y. Wang, Y. Xia, J. Mater. Chem. A **6**, 1443 (2018)
99. Y. Li, H. Dai, Chem. Soc. Rev. **43**, 5257 (2014)
100. H.F. Wang, Q. Xu, Matter **1**, 565 (2019)
101. D. Ji, L. Fan, L. Tao, Y. Sun, M. Li, G. Yang, T.Q. Tran, S. Ramakrishna, S. Guo, Angew. Chem. Int. Ed. **58**, 13840 (2019)
102. A. Wang, C. Zhao, M. Yu, W. Wang, Appl. Catal. B **281**, 119514 (2021)
103. A.I. Douka, Y. Xu, H. Yang, S. Zaman, Y. Yan, H. Liu, M.A. Salam, B.Y. Xia, Adv. Mater. **32**, e2002170 (2020)
104. W. Sun, F. Wang, B. Zhang, M. Zhang, V. Küpers, X. Ji, C. Theile, P. Bieker, K. Xu, C. Wang, M. Winter, Science **371**, 46 (2021)
105. D.U. Lee, J.-Y. Choi, K. Feng, H.W. Park, Z. Chen, Adv. Energy Mater. **4**, 1301389 (2014)
106. L. Ma, S. Chen, D. Wang, Q. Yang, F. Mo, G. Liang, N. Li, H. Zhang, J.A. Zapien, C. Zhi, Adv. Energy Mater. **9**, 1803046 (2019)
107. Y. Zhang, Y.-P. Deng, J. Wang, Y. Jiang, G. Cui, L. Shui, A. Yu, X. Wang, Z. Chen, Energy Storage Mater. **35**, 538 (2021)
108. C. Wang, W. Lu, Q. Lai, P. Xu, H. Zhang, X. Li, Adv. Mater. **31**, 1904690 (2019)
109. L. Gao, Z. Li, Y. Zou, S. Yin, P. Peng, Y. Shao, X. Liang, Science **23**, 101–348 (2020)
110. L. Li, L. Jiang, Y. Qing, Y. Zeng, Z. Zhang, L. Xiao, X. Lu, Y. Wu, J. Mater. Chem. A **8**, 565 (2020)
111. Y. Zeng, Y. Meng, Z. Lai, X. Zhang, M. Yu, P. Fang, M. Wu, Y. Tong, X. Lu, Adv. Mater. **29**, 1702698 (2017)
112. J. Liu, C. Guan, C. Zhou, Z. Fan, Q. Ke, G. Zhang, C. Liu, J. Wang, Adv. Mater. **28**, 8732 (2016)
113. H. Chen, Z. Shen, Z. Pan, Z. Kou, X. Liu, H. Zhang, Q. Gu, C. Guan, J. Wang, Adv. Sci. **6**, 1802002 (2019)
114. W. Zhou, D. Zhu, J. He, J. Li, H. Chen, Y. Chen, D. Chao, Energy Environ. Sci. **13**, 4157 (2020)
115. R. Wang, Y. Han, Z. Wang, J. Jiang, Y. Tong, X. Lu, Adv. Funct. Mater. **28**, 1802157 (2018)
116. C. Xu, J. Liao, C. Yang, R. Wang, D. Wu, P. Zou, Z. Lin, B. Li, F. Kang, C.-P. Wong, Nano Energy **30**, 900 (2016)
117. P. Hu, T. Wang, J. Zhao, C. Zhang, J. Ma, H. Du, X. Wang, G. Cui, ACS Appl. Mater. Interfaces **7**, 26396 (2015)
118. S.R. Ovshinsky, M.A. Fetcenko, J. Ross, Science **260**, 176 (1993)
119. Y.F. Liu, H.G. Pan, M.X. Gao, Q.D. Wang, J. Mater. Chem. **21**, 4743 (2011)
120. A. Schneemann, J.L. White, S. Kang, S. Jeong, L.W.F. Wan, E.S. Cho, T.W. Heo, D. Prendergast, J.J. Urban, B.C. Wood, M.D. Allendorf, V. Stavila, Chem. Rev. **118**, 10775 (2018)
121. G. Sandrock, J. Alloys Compd. **293–295**, 877 (1999)
122. C. Iwakura, K. Ohkawa, H. Senoh, H. Inoue, J. Electrochem. Soc. **149**, A462 (2002)

123. K. Kadir, T. Sakai, I. Uehara, J. Alloys Compd. **302**, 112 (2000)
124. K. Young, T. Ouchi, B. Huang, B. Chao, M.A. Fetcenko, L.A. Bendersky, K. Wang, C. Chiu, J. Alloys Compd. **506**, 841 (2010)
125. K. Young, R. Regmi, G. Lawes, T. Ouchi, B. Reichman, M.A. Fetcenko, A. Wu, J. Alloys Compd. **490**, 282 (2010)
126. S. Bliznakov, N. Drenchev, B. Drenchev, P. Delchev, P. Solsona, T. Spassov, J. Alloys Compd. **404**, 682 (2005)
127. C. Iwakura, H. Inoue, S.G. Zhang, S. Nohara, J. Alloys Compd. **270**, 142 (1998)
128. S. Nohara, N. Fujita, S.G. Zhang, H. Inoue, C. Iwakura, J. Alloys Compd. **267**, 76 (1998)
129. B. Sakintuna, F. Lamari-Darkrim, M. Hirscher, Int. J. Hydrogen Energy **32**, 1121 (2007)
130. G. Sandrock, J. Alloys Compd. **293**, 877 (1999)
131. X.Y. Zhao, L.Q. Ma, Y. Ding, M. Yang, X.D. Shen, Int. J. Hydrogen Energy **34**, 3506 (2009)
132. Y.F. Zhu, H.G. Pan, M.X. Gao, J.X. Ma, S.Q. Li, Q.D. Wang, Int. J. Hydrogen Energy **27**, 287 (2002)
133. Y.F. Zhu, H.G. Pan, G.Y. Wang, M.X. Gao, J.X. Ma, C.P. Chen, Q.D. Wang, Int. J. Hydrogen Energy **26**, 807 (2001)
134. E. Shangguan, J. Li, D. Guo, L. Guo, M. Nie, Z. Chang, X.-Z. Yuan, H. Wang, J. Power Sources **282**, 158 (2015)
135. A.B. Béléké, E. Higuchi, H. Inoue, M. Mizuhata, J. Power Sources **247**, 572 (2014)
136. W. Chen, Y. Jin, J. Zhao, N. Liu, Y. Cui, Proc. Natl. Acad. Sci. USA **115**, 11694 (2018)
137. Y. Liang, Y. Jing, S. Gheytani, K.-Y. Lee, P. Liu, A. Facchetti, Y. Yao, Nat. Mater. **16**, 841 (2017)